ASTROBIOLOGY
Volume 23, Number 5, 2023

DOI: 10.1089/ast.2022.0111

Environmental and Mineralogical Controls on Biosignature Preservation in Magnesium Carbonate Systems Analogous to Jezero Crater, Mars

Teanna M. Burnie,[1] Ian M. Power,[1] Carlos Paulo,[1] Hülya Alçiçek,[2] Luisa I. Falcón,[3] Yongjie Lin,[4,5] and Sasha Wilson[6]

Abstract

Jezero Crater on Mars is a paleolacustrine environment where Mg-carbonates may host evidence of ancient life. To elucidate the environmental and mineralogical controls on biosignature preservation, we examined samples from five terrestrial analogs: Lake Salda (Turkey), Lake Alchichica (Mexico), Qinghai-Tibetan Plateau (China), Mg-carbonate playas (British Columbia, Canada), and a mine with fine-grained ultramafic tailings (Yukon, Canada). The mineralogical compositions of the samples varied, yet were often dominated by either aragonite ($CaCO_3$) or hydromagnesite [$Mg_5(CO_3)_4(OH)_2 \cdot 4H_2O$]. Aragonite-rich samples from Alchichica, Mg-carbonate playas, and the ultramafic mine contained an abundance of entombed microbial biomass, including organic structures that resembled cells, whereas hydromagnesite-rich samples were devoid of microfossils. Aragonite often precipitates subaqueously where microbes thrive, thereby increasing the likelihood of biomass entombment, while hydrated Mg-carbonates typically form by evaporation in subaerial settings where biofilms are less prolific. Magnesite ($MgCO_3$), the most stable Mg-carbonate, forms extremely slowly, which may limit the capture of biosignatures. Hydrated Mg-carbonates are prone to transformation via coupled dissolution–precipitation reactions that may expose biosignatures to degradation. Although less abundant, aragonite is commonly found in Mg-carbonate environments and is a better medium for biosignature preservation due to its fast precipitation rates and relative stability, as well as its tendency to form subaqueously and lithify. Consequently, we propose that aragonite be considered a valuable exploration target on Mars. Key Words: Jezero Crater—Mars—Terrestrial analogs—Microbial fossils—Aragonite—Hydromagnesite. Astrobiology 23, 513–535.

1. Introduction

NASA's Mars 2020 mission is the first phase of a sample retrieval mission to return martian materials to Earth. The Perseverance rover's objectives include assessing the possibility of ancient life and collecting astrobiologically and geologically relevant samples to be cached and later transported to Earth for laboratory analyses (Farley *et al.,* 2020, 2022). Sample collection must prioritize targets with the greatest likelihood of containing biosignatures based on knowledge of terrestrial analogs due to a limited sample return capacity. Jezero Crater, the sampling location, was once filled with water as indicated by a fluvial inlet with a deltaic deposit, a river outlet on the opposite side of this ancient lake basin, and mineralogic evidence that includes phyllosilicates (Ehlmann *et al.,* 2008, 2010).

Based on orbiter data from the Mars Reconnaissance Orbiter's Compact Reconnaissance Imaging Spectrometer

[1]Trent School of the Environment, Trent University, Peterborough, Ontario, Canada.
[2]Department of Geology, Pamukkale University, Denizli, Turkey.
[3]Instituto de Ecología, Universidad Nacional Autónoma de Mexico, México DF, Mexico.
[4]Key Laboratory of Saline Lake Resources and Environments of Ministry of Natural Resources, Institute of Mineral Resource, Chinese Academy of Geological Sciences, Beijing, China.
[5]Department of Earth Sciences, University of Cambridge, Cambridge, United Kingdom.
[6]Department of Earth and Atmospheric Sciences, University of Alberta, Edmonton, Alberta, Canada.

for Mars (CRISM), this paleolacustrine environment contains magnesium carbonates among ultramafic materials (Ehlmann *et al.,* 2008; Goudge *et al.,* 2015; Tarnas *et al.,* 2021; Farley *et al.,* 2022).

Carbonates containing biosignatures are well documented on Earth (Riding, 2000), making those at Jezero Crater a priority target (Horgan *et al.,* 2020; Scheller *et al.,* 2021). CRISM data indicate that the strongest carbonate signatures are from the marginal carbonates that reside within the perceived littoral area of the paleolake basin (Ehlmann *et al.,* 2008; Horgan *et al.,* 2020; Zastrow and Glotch, 2021). The spectral signal of these carbonates resembles that of siderite ($FeCO_3$), magnesite ($MgCO_3$), and hydrated Mg-carbonates such as hydromagnesite [$Mg_5(CO_3)_4(OH)_2 \cdot 4H_2O$] (Ehlmann *et al.,* 2008; Horgan *et al.,* 2020; Zastrow and Glotch, 2021). If microbial life was present at Jezero during Mars' ancient past, it could have been preserved within carbonates, including the marginal carbonates. Furthermore, these carbonates may resemble microbial carbonate deposits such as microbialites or stromatolites (Westall *et al.,* 2015; Horgan *et al.,* 2020), which provide some of the oldest evidence of life on Earth (Walsh, 1992; Noffke *et al.,* 2013; Hickman-Lewis *et al.,* 2018).

Microbial carbonates, that is, deposits formed through microbial activity, have been an important part of Earth's geologic record since the Archean and form in a wide range of environments in addition to marine settings, including lakes, springs, caves, soils, and playas (Riding, 2000). Authigenic carbonates often form in association with microbes with the potential to preserve biosignatures (Riding, 2000; Dupraz *et al.,* 2009; Robles-Fernández *et al.,* 2022). Evidence for marginal carbonates (Balci *et al.,* 2020; Horgan *et al.,* 2020) and of a paleolacustrine environment (Ehlmann *et al.,* 2008) offers a robust contextual basis to argue the probability of microbial carbonates existing on Mars. Among the oldest fossils on Earth are calcium carbonate stromatolites formed in a shallow marine environment dating to $\sim$3.5 Ga (Allwood *et al.,* 2007, 2018; Sugitani *et al.,* 2010). In contrast, the marginal carbonates at Jezero are suspected to be magnesium carbonates, resulting from the weathering of the crater's ultramafic (Mg-rich) bedrock (Horgan *et al.,* 2020; Tarnas *et al.,* 2021). In addition, Perseverance has detected magnesium–iron carbonates on the floor of Jezero Crater, likely having formed from *in situ* olivine carbonation (Farley *et al.,* 2022). However, the preservation of biosignatures in Mg-carbonates has been underexplored due to their lower abundance on Earth compared with Ca-carbonates.

The current understanding of Mg-carbonate minerals indicates that they are likely a poor medium for entombing biomass, thereby reducing the likelihood of biosignature preservation (Power *et al.,* 2007, 2009, 2014, 2019). Research from Mg-rich environments on Earth, analogous to Jezero Crater, shows that magnesite is slow to precipitate at Earth's surface conditions and that hydrated Mg-carbonates (*e.g.,* hydromagnesite) are prone to transformation (Power *et al.,* 2019; Harrison *et al.,* 2021). However, the calcium carbonate mineral aragonite ($CaCO_3$) is often found in sedimentary systems dominated by Mg-carbonates. We propose that aragonite is a better preservation medium than Mg-carbonate minerals within the Mg-carbonate depositional environments that are analogous to Jezero Crater.

This study examines carbonate microbialite and sediment samples from five terrestrial analogs to determine dominant mineralogy, assess formation conditions, and describe entombed biomass that has either become fossilized or has the potential to do so. We elucidate the environmental and mineralogical controls that influence the likelihood of microbial biomass being encapsulated within carbonate minerals. The relationship between carbonate mineral species and biosignature abundance will inform the selection of ideal targets for the sample caching mission on Mars.

2. Field Site Descriptions and Sampling

Jezero Crater (45-km diameter) is a paleolacustrine system thought to have been active until the Early Hesperian era (3.5 Ga) (Goudge *et al.,* 2018). The area is characterized by mafic and ultramafic spectral signatures, a closed basin structure, and a limited elevation zone containing distinct marginal carbonates. These features indicate that carbonate formation may have occurred at the evaporative margin from Mg-rich, alkaline waters in the littoral zone of the paleolake (Horgan *et al.,* 2020). The investigation of martian magnesium carbonates will be aided by an improved understanding of the environmental and mineralogical controls on the preservation of biosignatures within these minerals on Earth (Scheller *et al.,* 2021).

Terrestrial analogs for Mg-carbonate littoral deposits include Lake Salda, Turkey (Fig. 1A) (Balci *et al.,* 2020; Russell *et al.,* 1999), the crater lake of Alchichica, Mexico (Fig. 1B) (Kaźmierczak *et al.,* 2011), and sites on the Qinghai-Tibetan Plateau, including Dujiali Lake (Fig. 1C, D) (Lin *et al.,* 2017) and Qaidam Basin (Fig. 1E). The martian carbonates may also have formed from springs or locations where groundwaters discharged and evaporated. Potential analogs for this mode of formation include the Mg-carbonate playas in British Columbia, Canada (Fig. 1F) (Power *et al.,* 2014), where aragonite rubble is found among mounds of Mg-carbonate sediments (Fig. 1G).

Other possible modes of carbonate formation are the weathering of fine-grained ultramafics (*e.g.,* ash or sediment) and deposition within smaller isolated ponds. At the Clinton Creek chrysotile mine, fine-grained serpentinite tailings have weathered over several decades causing the formation of Mg-carbonate efflorescences (Fig. 1H) (Wilson *et al.,* 2009), while aragonite microbialites have formed within the open pit pond (Fig. 1I) (Power *et al.,* 2011). These five modern terrestrial analogs provide an opportunity to study microbial biomass entombment and biosignature preservation within Mg-carbonates and aragonite over a wide range of environmental conditions.

2.1. Lake Salda

Lake Salda in southwestern Turkey (37°32′43.7″N, 29°40′59.8″E) is a large midlatitude lake fed by small ephemeral streams and has an average depth of 80 m (Shirokova *et al.,* 2013). The lake is a closed-basin system for most of the year (Braithwaite and Zedef, 1996; Balci *et al.,* 2020). The pH ranges from 8 to 10, and the [Mg^{2+}]/[Ca^{2+}] ratio fluctuates seasonally and with depth (Kazanci *et al.,* 2004). Ultramafic rocks underlie most of the basin, providing a source of Mg and alkalinity to the lake waters. The evaporation of Mg-rich waters along the near-shore

FIG. 1. Photographs of Mg-carbonate depositional environments that are analogous to Jezero Crater, Mars. **(A)** Hydromagnesite tufas or microbialites at Lake Salda, Burdur, Turkey (measuring tape for scale). **(B)** Aragonite/hydromagnesite microbialites at the crater lake of Alchichica, Puebla, Mexico. Frozen Dujiali Lake **(C)** with hydromagnesite sediments along its shoreline **(D)**, and aragonite ooids **(E)** that are found along the paleo-shoreline of Qaidam Basin, Qinghai-Tibet Plateau. **(F)** Hydromagnesite–magnesite playas of Atlin, British Columbia, Canada, where aragonite rubble (trowel for scale) lays among hydromagnesite mounds **(G)**. **(H)** Clinton Creek asbestos tailings (Yukon, Canada) cemented by hydrated Mg-carbonate efflorescences that formed from *in situ* weathering. **(I)** The open pit pond at the Clinton Creek mine that contains aragonite microbialites (inset; marker for scale). Color images are available online.

environment causes Mg-carbonate minerals, mainly hydromagnesite, to precipitate. Although the structures are often referred to as microbialites (Russell *et al.,* 1999; Shirokova *et al.,* 2013; Balci *et al.,* 2020), it may be more accurate to call them tufa deposits.

Tufas mounds and columns form from carbonate precipitation in ambient air, such as those at Mono Lake, California, United States (Council and Bennett, 1993). Kazanci *et al.* (2004) state that the stromatolites in Lake Salda formed through the entrapment of littoral sediments and diatoms within algal mats, developing mounds reaching 10–30 cm in diameter. Mildly consolidated carbonate samples (hand specimen size) were collected from three terraces along the exposed southwestern shore of Lake Salda (Fig. 1A).

2.2. Lake Alchichica

Lake Alchichica (19°24′46.0″N, 97°24′10.3″W) is a crater lake at an altitude of 2300 m above sea level in the Central Mexican Plateau, Mexico, a region classified as a ''cold-desert'' (Kaźmierczak *et al.,* 2011; Gérard *et al.,* 2013; Valdespino-Castillo *et al.,* 2014). The crater basin is bowl-shaped, reaching a maximum depth of ~60 m, with an asymmetrical ring of microbialites surrounding the periphery (Fig. 1B) (Kaźmierczak *et al.,* 2011). The lake is a closed basin fed by precipitation and groundwater infiltration and is defined as a soda lake due to its salinity and alkalinity (pH ~9.5) (Valdespino-Castillo *et al.,* 2014). Although calcareous mountains border the lake, the calcium concentration is low, resulting in a high $[Mg^{2+}]/[Ca^{2+}]$ ratio (Kaźmierczak *et al.,* 2011). Hydromagnesite precipitation is favored under these conditions; however, the marginal microbialites contain both hydromagnesite and aragonite (Gérard *et al.,* 2013).

There are two types of discontinuous microbialites along the margin of Lake Alchichica, and they are categorized as mound-type (white) and columnar-type (brown) based on the differences in morphology, mineralogy, texture, isotopic signatures, and microbial composition (Tavera and Komárek, 1996; Kaźmierczak *et al.,* 2011). Both microbialite types were examined in this study (Fig. 1B). The white microbialites are irregular mounds with macroscopic laminations and are hydromagnesite-dominated, whereas the brown microbialites are aragonite-dominated and develop as chimney-like structures that are macroscopically nonlaminated and porous (Kaźmierczak *et al.,* 2011). Of the five sample locations for terrestrial analogs, this site is the only crater lake akin to the formation of the paleolake basin of Jezero Crater.

2.3. Qinghai-Tibet Plateau

Dujiali Lake (Fig. 1C) is an alkaline lake in the central Qinghai-Tibet Plateau (32°01′43.4″N, 88°38′31.6″E) at an altitude of 4524 m above sea level. The lake was dry in the 1980s, and the present water and solute mass have accumulated due to increased precipitation and meltwater (Lin *et al.,* 2017 and references therein). The lake has a surface area of 80 km^2 and is ~3 m deep (Lin *et al.,* 2017). Hydromagnesite deposits are widely distributed as bands around the lake margins and as sediments within the lake, which are thought to have periodically dried to form a playa during the Holocene.

Today, the hydromagnesite sediments can only be observed in the first terrace in the northwest due to the rise of lake waters. The sediment samples for this study were collected from this terrace (Fig. 1D) and were bright white after removal of the brown and clay-like weathered surface crust (Lin *et al.,* 2017, 2019a, 2019b). Lin *et al.* (2017) proposed that these hydromagnesite deposits are authigenic, having crystallized from the evaporation of lake water.

The Qaidam Basin on the Qinghai-Tibetan Plateau (NW China) has been studied as a terrestrial analog for Mars research (Xiao *et al.,* 2017). The plateau is one of the driest deserts on Earth and is considered an analog to the playas and lakes of ancient Mars. Qaidam Basin is the largest intermontane sedimentary basin with an area of ~120,000 km^2 and an average elevation of ~3000 m above sea level (Xiao *et al.,* 2017). Holocene lacustrine carbonate ooids are present in the playas of the western Qaidam Basin (Sun *et al.,* 2019).

The ooids (Fig. 1E) for this study were collected from the surface in the Honggouzi section (38°27′43.12″N, 91°16′47.93″E), northwest of the Qaidam Basin, which is currently overlaid by a chemical-eolian deposit and underlaid by the lake sediments that include clays, carbonate, and evaporite salts. The ooids were well preserved with no apparent diagenetic alterations and have been described in detail by Lin *et al.* (2022).

2.4. Atlin playas

The Mg-carbonate playas near Atlin, British Columbia, Canada (59°34′23.1″N, 133°41′45.3″W) reside in a region characterized by a dry subarctic climate (Fig. 1F). The playas are mainly composed of hydromagnesite and magnesite that have formed through evaporation of Mg-HCO_3 groundwater (Power *et al.,* 2007). Radiocarbon dating suggests that Mg-carbonate deposition has been occurring for the last 8000 years (Power *et al.,* 2014). The Jezero paleolake is thought to have become a closed basin as the planet-wide water budget declined (Clifford and Parker, 2001), in which a playa-like environment may have formed the light-toned floor of the crater (Salese *et al.,* 2019).

In this case, hydromagnesite–magnesite playas such as those in British Columbia (Renaut, 1993; Power *et al.,* 2014) are a suitable terrestrial analog (Power *et al.,* 2009). It is possible that the geochemical conditions that existed at Jezero Crater following the end of fluvial activity (~3.7 Ga) are comparable with the conditions currently found at the playas (Fassett and Head, 2005; Horgan *et al.,* 2020). The Mg-carbonate sediments near Atlin are not lithified, and there is no clear indication that morphological biosignatures are being preserved within them (Power *et al.,* 2007, 2009, 2014, 2019). However, this was the site where cyanobacterially induced precipitation of the Mg-carbonate mineral, dypingite $[Mg_5(CO_3)_4(OH)_2 \cdot \sim 5H_2O]$, was first documented (Power *et al.,* 2007).

This study focused on lithified aragonite samples collected from piles of rubble. Aragonite precipitates in the main wetland of the southeastern playa (Fig. 1F), where microbial mats thrive (Power *et al.,* 2007, 2009). These sediments lithify along the wetland periphery and, over time, may pile together by the lateral growth of hydromagnesite mounds or formation of patterned ground via frost heave

(Fig. 1G) (Power *et al.,* 2014; Power *et al.,* 2009). Microbialite and pisolite hand specimens (10s cm in size) were collected from the playa and were previously described by Power *et al.* (2009) at the macroscopic scale. The pisolite collected comprised pisoids with inverse-graded bedding. Some of the microbialites display alveolar-septal structures, solidified by aragonite precipitation (Power *et al.,* 2007, 2009).

2.5. Clinton Creek chrysotile mine

The abandoned Clinton Creek asbestos mine (64°26′57.6″N, 140°42′21.2″W) is located in the Canadian subarctic, 77 km northwest of Dawson City, Yukon (Power *et al.,* 2011). This site was selected due to the presence of hydrated Mg-carbonates formed from subaerial weathering of fine-grained ultramafics (*e.g.,* tailings) and aragonite microbialites along the rim of the open pit pond (Wilson *et al.,* 2009; Power *et al.,* 2011; White *et al.,* 2015). Likewise, the ultramafic signatures at Jezero Crater may be consistent with the properties of an ultramafic, fine-grained tephra deposit that would be susceptible to subaerial weathering (Horgan *et al.,* 2020). The tailings may also be comparable with ultramafic sediments deposited in alluvial fans on the western side of the Jezero Basin.

Spectral data collected from the detrital fan deposits have shown strong olivine and carbonate signatures overlying smectite layers (Horgan *et al.*, 2020). Furthermore, Farley *et al.* (2022) postulated that magnesium–iron carbonates detected by Perseverance in the Séítah formation on the crater's floor formed from *in situ* olivine carbonation. *In situ* carbonation of fine-grained ultramafic material at Earth's surface is rare, making the historic chrysotile tailings a unique analog site.

Two subenvironments at the mine were investigated: the ultramafic asbestos tailings and the open pit pond. The tailings have been exposed to weathering since at least 1978 when the mine closed. Their high surface area from the milling process facilitates *in situ* Mg-carbonate mineralization, resulting in carbonate efflorescences composed of the hydrated Mg-carbonate phases lansfordite ($MgCO_3 \cdot 5H_2O$), nesquehonite ($MgCO_3 \cdot 3H_2O$), dypingite, and hydromagnesite that cement the tailings (Fig. 1H) (Wilson *et al.,* 2009).

Microbialites composed of aragonite are present in the open pit pond (Fig. 1I, inset) and are one of the fastest growing and northern-most microbialite communities discovered (Power *et al.,* 2011). The pond does not have any inlets or outlets and, thus, is susceptible to evapoconcentration. The microbialites have a columnar form, are up to 15 cm in height (Power *et al.,* 2011), and contain detritus incorporated into the biofilms and carbonate structures. The Clinton Creek mine offers an opportunity to study aragonite microbialites in an ultramafic setting.

3. Materials and Methods

3.1. Mineralogical characterization

Samples were characterized by a powdered X-ray diffractometer (XRD) at Trent University. A McCrone micronizing mill was used to micronize subsamples (2.0 g) for 7 min in pure anhydrous ethanol with agate grinding elements. Before XRD analysis, samples were dried under laboratory conditions and disaggregated with an agate mortar and pestle. Powders were mounted in back-loading holders to minimize preferred orientation. Diffraction patterns were collected by a Bruker D2 Phaser diffractometer with a 0.02-step size over a range of 5°–80° 2θ at 4 s/step with a 15-rpm spin. The diffractometer was equipped with a LYNXEYE XE-T position-sensitive detector and incident and diffracted beam Soller slits. A fine-focus Cu X-ray tube using a 6° take-off angle was operated at 30 kV, and 10 mA was used to generate X-rays. Mineral-phase identification was conducted with the DIFFRAC.EVA Version 5 XRD-phase analysis software (Bruker).

Quantitative analysis of the phases was performed by using Rietveld refinement with XRD data to provide a weight-percent (wt %) measurement of the respective phases (Rietveld, 1969; Hill and Howard, 1987; Bish and Howard, 1988). These refinements were conducted using TOPAS Version 6 software (Bruker), and crystal structure data were obtained from the International Center for Diffraction Data Powder Diffraction File 2 2020 database (ICDD PDF2).

3.2. Light and electron microscopy

Hand specimens were examined with a Zeiss SteREO Discovery V20 stereomicroscope and PlanAchromat S objective (1.0 × f/Reo; WD = 81 mm). Polished thin sections (27 × 46 mm) of the samples were made by Vancouver Petrographics Ltd. (Langley, BC, Canada) and examined under plane- and cross-polarized light with a Zeiss Axioscope 5 microscope equipped with a Colibri 5, Type RGB-UV 4-channel fluorescence light source. Images of the samples were collected with an Axiocam 208 color camera.

For electron microscopy, subsamples of the hand specimens were embedded by using Buehler EpoThin™ 2 epoxy resin and hardener and polished with a Buehler EcoMet™ 30 manual single-grinder polisher. The final polish was performed using a TriDent™ pad and MasterPrep™ diamond suspension (0.05 μm) to create a glass-like surface. Duplicate samples were acid-etched to reveal entombed biomass below the carbonate surface. The embedded samples were exposed to an acid treatment of 1% HCl solution for 3 min, followed by a rinse with deionized water containing 2% glutaraldehyde and 0.85% NaCl for 30 min (Power *et al.,* 2011). Samples were subsequently dehydrated to preserve biogenic material using an ethanol series (70%, 90%, and 100% × 3 for 15 min each), followed by a 1:1 hexamethyldisilazane (HMDS) to anhydrous ethanol bath for 10 min, and finally submerged for 20 min in a bath of 100% HMDS (Preston *et al.,* 2011).

All samples were coated using a Filgen osmium coater (OPC 80T) that applied 10 nm of osmium metal to the sample surface to improve conductivity. The samples were secured to the microscope stage with 12 mm carbon adhesive tabs and copper tape to eliminate charging effects. Scanning electron microscopy (SEM) was performed at The University of Western Ontario at the Nanofabrication Facility in London, Ontario, Canada. The LEO 1540 XB field emission SEM collected high-resolution micrographs at an operating voltage of 1.0 kV with a secondary electron detector and a quadrant backscatter detector operating at

20 kV. Elemental analysis was performed with an Oxford Instruments X-Max energy dispersive spectrometer (EDS) at 20 kV.

3.3. Geochemical modeling

The saturation indices (SIs) of relevant carbonate minerals were determined with PHREEQC V3 (Parkhurst and Appelo, 2013) using the llnl.dat thermodynamic database compiled at the Lawrence Livermore National Laboratory, which was modified to include thermodynamic data for dypingite formation at 25°C and 35°C obtained by Harrison *et al.* (2019). Geochemical modeling was performed at a constant temperature (*e.g.,* 25°C) and using the water composition (pH, major cations, and anions) previously reported for the field sites (Power *et al.,* 2010, 2011, 2014; Kaźmierczak *et al.,* 2011; Lin *et al.,* 2017; Balci *et al.,* 2020).

PHREEQC was also used to simulate the effect of evaporation on the SI values for carbonate minerals for waters in equilibrium with atmospheric CO_2 ($pCO_2 = 10^{-3.4}$ atm). Parkhurst and Appelo (2013) described the code used in these simulations that concentrate 1.0 L of water by sequentially removing a fixed number of moles to simulate an irreversible reaction where water is lost from the chemical system. The effect of removing 52.73 mol in 19 steps, or the equivalent of 95% water removal, was evaluated for the waters from the analog sites. In addition, the SIs calculated before and after evaporation simulations were compared, and changes in these values were used as indicators for favorable conditions (SI >0) for the precipitation of Ca- and Mg-carbonate minerals.

3.4. Stable isotopes

Carbonate samples were analyzed for their stable carbon and oxygen isotopes at the Ján Veizer Stable Isotope Laboratory in Ottawa, Canada. Samples were loaded into exetainers and reacted with 0.1 mL of H_3PO_4 (S.G. 1.91). The exetainers were then capped and helium-flushed while horizontal. Samples containing calcite were reacted at 25°C for 24 h and samples containing magnesium carbonate minerals were reacted at 70°C for 4 h. Measurements were performed on a Delta XP Isotope Ratio Mass Spectrometer and a Gas Bench II, both from Thermo Finnigan, with an analytical precision (2 sigma) of ±0.1‰. The stable carbon and oxygen isotope values are reported in the conventional δ notation in per mil (‰) relative to Vienna Pee Dee Belemnite (VPDB) and Vienna Standard Mean Ocean Water (VSMOW), respectively.

4. Results

4.1. Water chemistry and carbonate precipitation

Mineral SIs were used to predict the precipitation of relevant carbonate minerals and to compare with XRD results. The waters from Lake Salda were saturated in all six carbonate minerals of interest: magnesite, hydromagnesite, dypingite, nesquehonite, calcite, and aragonite. This site is the only one with waters saturated with respect to nesquehonite, although marginally (SI = 0.1). In addition, it had the highest SIs for hydromagnesite (5.1), dypingite (3.8), and magnesite (2.6). The pH was 9.4 and the Mg/Ca molar ratio was 36.0 (Table 1). The Lake Salda samples were predominately hydromagnesite (96 wt %) with minor amounts of aragonite (4 wt %; Table 2), which is consistent with PHREEQC modeling predictions. Trace halite was detected by SEM and EDS.

The Mg/Ca molar ratio of the Alchichica lake surface waters is similar to that of Lake Salda (37.8); however, the pH is slightly lower (8.9) with considerably lower alkalinity (720 mg HCO_3/L). The microbialites from Lake Alchichica were the only samples containing major abundances (≥10 wt %) of both hydromagnesite and aragonite. The white microbialite contained a higher proportion of hydromagnesite than aragonite, 83 wt % and 17 wt %, respectively, compared with the brown microbialite (aragonite = 89 wt % and hydromagnesite = 11 wt %; Table 2). The lake water is saturated with respect to hydromagnesite (SI = 2.9) and aragonite (SI = 1.0; Table 1).

Dujiali Lake has an average pH of 9.6, alkalinity of 320 mg HCO_3/L, and Ca and Mg concentrations of 9.6 and 42.4 mg/L, respectively, with a Mg/Ca molar ratio of 7 (Table 1). These waters are undersaturated with respect to hydromagnesite (SI = −1.1) yet supersaturated with respect to aragonite (SI = 0.6). The terrace sediments along the lake's margins contained 96 wt % hydromagnesite and 4 wt % aragonite (Table 2). No water was associated with the Qaidam ooids, which were composed of 97 wt % aragonite and 3 wt % quartz.

Two distinct water sources in the Atlin playas were considered, water from the water table within the hydromagnesite–magnesite mounds and an isolated pond where aragonite forms (Power *et al.,* 2014). The water from the mounds had a pH of 8.0 and the highest Mg/Ca molar ratio of the entire data set (1217). These waters were saturated with respect to lansfordite, magnesite (SI = 2.4), and hydromagnesite (SI = 1.1; Table 1). A hardpan at the water table forms due to lansfordite precipitation; however, the majority of the Mg-carbonate sediments are mixtures of hydromagnesite and magnesite (Power *et al.,* 2014). The isolated pond had a lower pH of 7.5 and a relatively low Mg/Ca molar ratio of 19.4 (Table 1).

Power *et al.* (2014) proposed that the aragonite rubble (Fig. 1G) forms from isolated ponds ($SI_{arg} = 0.8$) or along the main wetland periphery where aragonite precipitation dominates. The microbialite and pisolite entirely comprised aragonite (100 wt %; Table 2), consistent with PHREEQC modeling predictions.

The Clinton Creek tailings puddle had the second-highest Mg/Ca molar ratio (183) of all the waters examined. Similar to the Atlin mound groundwater, it was not saturated with respect to calcite or aragonite (Table 1). Puddles on the tailings are thought to have formed from waters percolating through the tailings and collecting at low points. Therefore, these puddles may represent pore waters from which the efflorescences have precipitated. Although PHREEQC modeling predicts hydromagnesite (SI = 1.6) precipitation, evaporation of 40% and 95% would be required to precipitate dypingite and nesquehonite, which are also found within efflorescences (Wilson *et al.,* 2009).

The second water sampled from Clinton Creek was the open pit pond where the microbialites were collected. The pond has a pH of 8.4 and Mg/Ca molar ratio of 6.0. Although the waters are saturated with respect to magnesite,

Table 1. Water Chemistry and Saturation Indices for Select Carbonates

Site	*pH*	*[Ca], mg/L*	*[Mg], mg/L*	*Mg/Ca molar ratio*	*Alkalinity, mg HCO_3/L*	*Saturation indices*
Lake Salda, SW shore[a]	9.4	17.8	388.1	36.0	2038	Sat.: Hmgs* (5.1), dyp (3.8), mgs (2.6), cal (1.6), arg* (1.4), nes (0.1)
Lake of Alchichica, surface waters[b]	8.9	20.0	458.0	37.8	720	Sat.: Hmgs* (2.9), mgs (2.4), cal (1.1), arg* (1.0), dyp (0.6) Unsat.: Nes (−0.7)
Dujiali Lake[c]	9.6	9.6	42.4	7.0	320	Sat. Mgs (1.2), cal (0.8), arg* (0.6) Unsat.: Hmgs* (−1.1), nes (−1.8)
No water associated with Qaidam Basin ooids						
Atlin playas, mound groundwater[d]	8.0	2.1	1550.0	1217.1	8480	Sat.: Mgs* (2.4), hmgs* (1.1) Unsat.: Cal (−0.1), arg (−0.2), dyp (−0.4), nes (−0.7)
Atlin playas, isolated ponds[d]	7.5	68.1	800.0	19.4	5150	Sat.: Mgs (1.6), cal (0.9), arg* (0.8) Unsat.: Nes (−1.5), hmgs (−3.1), dyp (−4.6)
Clinton Creek, tailings puddle[e]	9.5	1.4	155.9	183.6	358	Sat.: Mgs (1.8), hmgs* (1.6) Unsat.: Cal (−0.1), arg (−0.2), dyp* (−0.8), nes* (−1.3)
Clinton Creek, open pit pond[f]	8.4	95.7	350.0	6.0	243	Sat.: Mgs (1.0), cal (0.7), arg* (0.6) Unsat.: Nes (−2.2), hmgs (−4.3), dyp (−5.8)

Saturation indices were determined for magnesite (mgs), hydromagnesite (hmgs), dypingite (dyp), nesquehonite (nes), calcite (cal), and aragonite (arg) and are grouped into those saturated (Sat.) and undersaturated (Unsat.) in site waters. Minerals identified in the corresponding solid samples (Table 2) are denoted with an asterisk.

[a]The water chemistry data are from Balci *et al.* (2020; SLW5).
[b]The water chemistry data are from Kazmierczak *et al.* (2011).
[c]The water chemistry data are from Lin *et al.* (2017).
[d]The water chemistry data are from Power *et al.* (2014).
[e]The water chemistry data are from Power *et al.* (2010).
[f]The water chemistry data are from Power *et al.* (2011).

calcite, and aragonite (Table 1), the microbialite samples comprised aragonite (66 wt %), lizardite [$Mg_3Si_2O_5(OH)_4$] (16 wt %), quartz (SiO_2; 10 wt %), and muscovite [$KAl_2(AlSi_3O_{10})(OH)_2$] (8 wt %; Table 2). While aragonite (SI = 0.6) precipitation is consistent with PHREEQC modeling, the silicate minerals are present as detrital grains.

The stable carbon and oxygen isotopic compositions of the carbonate minerals provide insights into the environmental conditions under which they formed (Fig. 2). The Lake Salda hydromagnesite stromatolite and Dujiali Lake hydromagnesite sediments had similar $\delta^{13}C$ and $\delta^{18}O$ values of 4.9‰ and 5.9 ± 0.5‰ VPDB and 36.3‰ and 35.6 ± 0.4‰ VSMOW, respectively. The isotopic data for the Dujiali sediments are provided by Lin *et al.* (2017) ($n = 7$). The Qaidam Basin aragonite ooids had $\delta^{13}C$ and $\delta^{18}O$ values of 4.4‰ and 36.0‰, respectively. The Alchichica white (hmgs-rich) and brown (arg-rich) microbialites had distinctly different $\delta^{13}C$ values of 7.2‰ and 3.3‰, and $\delta^{18}O$ values of 36.1‰ and 29.6‰, respectively. The Atlin surface hydromagnesite–magnesite sediments had $\delta^{13}C$ and $\delta^{18}O$ values of 6.9 ± 0.9‰ and 18.8 ± 0.7‰, respectively (Power *et al.,* 2014; $n = 7$). Distinct from these sediments, the aragonite microbialite and pisolite had $\delta^{13}C$ values of 4.5‰ and 4.8‰, and $\delta^{18}O$ values of 12.2‰ and 12.6‰, respectively. The Clinton Creek Mg-carbonate efflorescences had $\delta^{13}C$ and $\delta^{18}O$ values of 10.9 ± 2.3‰ and 23.6 ± 1.4‰ (Wilson *et al.,* 2009; $n = 18$), which were distinct from the aragonite microbialites that had values of −5.0 ± 0.6‰ and 14.8 ± 0.2‰, respectively (Power *et al.,* 2011; $n = 36$). Average isotope values for all samples are plotted in Fig. 2.

4.2. Entombed biomass and morphological biosignatures

Our study of the field samples focused on imaging entombed biomass that has been mineralized with an emphasis on comparing hydromagnesite- and aragonite-rich samples. We define entombed biomass as microbial remnants, including diatom frustules, organic structures resembling microbes, and amorphous organics that have become encapsulated by minerals (Cady *et al.,* 2003; Power *et al.,* 2011; Lepot *et al.,* 2014; Alleon *et al.,* 2016; McCutcheon *et al.,* 2016; Tait *et al.,* 2017, 2022). This entombed biomass may result in microfossil preservation or leave behind other types of biosignatures (*e.g.,* biomolecules). The aragonite-rich samples, including the Alchichica brown microbialite, Atlin microbialite and pisolite, and Clinton Creek microbialites, contained the greatest abundance of entombed biomass and morphological structures interpreted as fossilized microbes. The key observations from light and electron microscopy are summarized in Table 2.

4.2.1. Lake Salda microbialites. The Lake Salda microbialite sample, or a more descriptive term may be tufa, was fragile, primarily white, and devoid of organic matter (Fig. 3A). Entombed biomass or microfossils were absent from this sample, which contained one of the highest

Table 2. Environment, Quantitative Mineralogy, and Key Observations of Samples

Site	*Sample*	*Subenvironment*	*Mineralogy, wt %*	*Observations*
Lake Salda (Fig. 3)	Stromatolite/tufa	Subaerial shoreline	Hmgs (96), arg (4)	Consolidated not lithified, white granular texture. Trace halite identified using SEM. Fine laminations but no entombed biomass or microfossils found within hmgs or arg.
Lake Alchichica (Fig. 4)	White microbialite	Intertidal, shoreline	Hmgs (83), arg (17)	Thick white lithified layers of granular material with iron-staining. Spherical microfossils with iron oxides in the arg. Hmgs mostly lacked entombed biomass.
	Brown microbialite	Intertidal, shoreline	Arg (89), hmgs (11)	White dome-shaped crusts with brown and iron-stained material. Two tube-like features 2 mm in diameter seen in hand specimen. Diatom frustules, organic filaments, and spheres, interpreted as microbial remnants found in arg.
Dujiali Lake (Fig. 5)	Hmgs sediments	Subaerial shoreline	Hmgs (96), arg (4)	Unconsolidated sediments lacking in biomass and biosignatures. Hmgs has rosette and platy morphologies.
Qaidam Basin	Ooids	Paleo-shoreline	Arg (97), qtz (3)	Ooids (diameter = 200–600 μm) are well preserved, that is, no diagenetic alterations. No entombed biomass or microfossils present.
Atlin playas (Fig. 6)	Hmgs-mgs sediments	Subaerial mounds	Mixtures of hmgs and mgs	Unconsolidated white muddy sediments. Filamentous cyanobacteria live on some surfaces but are not preserved.
	Microbialite	Subaqueous, isolated pond or pond peripheries	Arg (100)	Beige to reddish color with alveolar-septal structure seen in hand specimen. Linear laminations containing cell membranes, diatom frustules, and filamentous and spherical structures, interpreted as microbial remnants.
	Pisolite	Subaerial/subaqueous (vadose zone)	Arg (100)	Beige color, inverse graded bedding, 2–10-mm-diameter pisoids. Concentric laminations encasing diatoms frustules, organic spheres, and filaments, interpreted as microbial remnants.
Clinton Creek tailings pile (Fig. 7)	Mg-carbonate efflorescences	Subaerial, *in situ* weathering	Hydrated Mg-carbonates (100)	Efflorescences contained a mixture of hydromagnesite, dypingite, and nesquehonite. Entombed biomass was not seen in these samples.
Open pit pond	Microbialite	Subaqueous shoreline	Arg (66), lz (16), qtz (10), ms (8)	Gray with a clotted texture and entrapped granular fragments. Micritic thrombolite-like texture containing diatom frustules, and microbial biomass that fluoresces under UV light.

Minerals found in samples included hydromagnesite (hmgs) and aragonite (arg), and lizardite (lz) and muscovite in the Clinton Creek microbialites. Abundances (wt %) are based on Rietveld refinement using XRD data.

SEM = scanning electron microscopy; UV = ultraviolet; XRD = X-ray diffractometer.

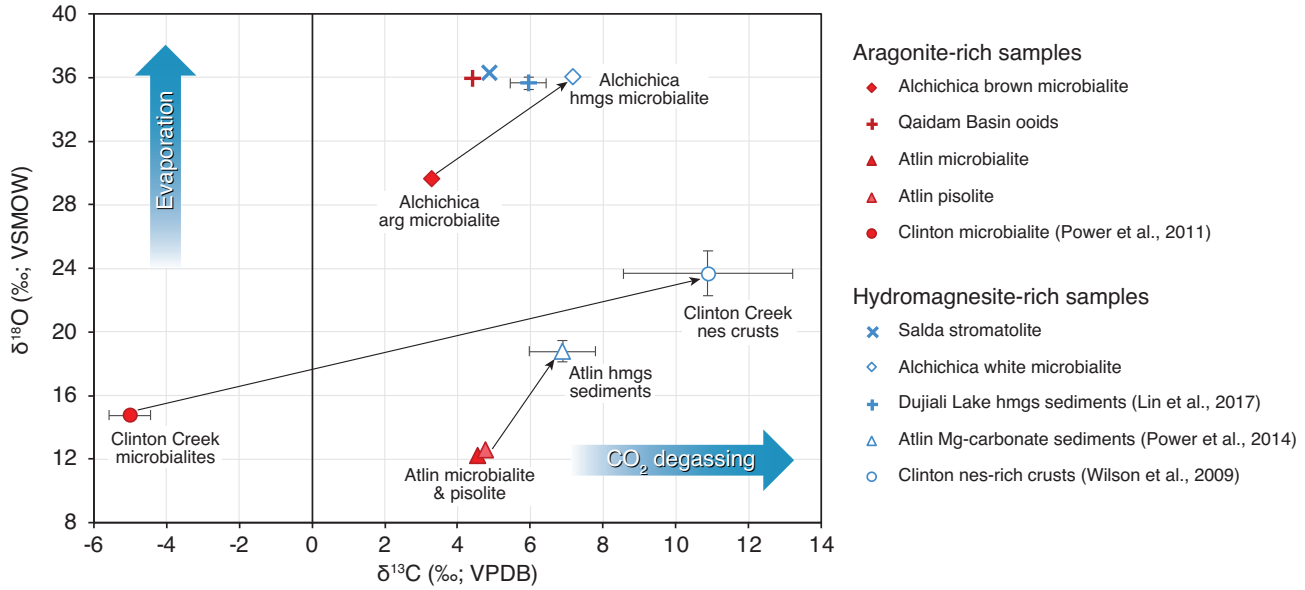

FIG. 2. Stable carbon and oxygen isotopic compositions of carbonate samples from the terrestrial analogs. Data are plotted as $\delta^{13}C$ and $\delta^{18}O$ values in per mil relative to VPDB and VSMOW, respectively. Sites with both hydromagnesite-rich (blue symbols) and aragonite-rich (red symbols) samples are connected by arrows. Evaporation and CO_2 degassing cause enrichment of ^{18}O and ^{13}C in authigenic carbonates. VPDB = Vienna Pee Dee Belemnite; VSMOW = Vienna Standard Mean Ocean Water. Color images are available online.

abundances of hydromagnesite (96 wt %) among the samples. There were no recognizable microfossils in this sample when viewed with light microscopy; however, laminations characteristic of stromatolites were visible in small areas of the polished thin section. Although stromatolitic laminations may form from microbial activity (Kennard and James, 1986; Schopf *et al.,* 2007), this texture may also develop via physical and chemical processes (Grotzinger and Rothman, 1996; Grotzinger and Knoll, 1999). The hydromagnesite also appeared devoid of any entombed biomass when viewed using SEM (Fig. 3B).

Acid etching revealed the platy crystal morphology of the hydromagnesite but did not uncover any observable organics or biomass. Although there was minor aragonite (4 wt %) in the Lake Salda sample, it also lacked structures resembling microfossils (Fig. 3B). The presence of halite strongly indicates that this sample was exposed to subaerial conditions where evapoconcentration of Lake Salda water caused precipitation of this halide mineral. In one area, both hydromagnesite and aragonite were near halite (Fig. 3B). However, the abundance of halite was insufficient to be detected by XRD. The Supplementary Information contains additional micrographs of the Lake Salda sample showing the hydromagnesite and aragonite lacking recognizable entombed biomass or microfossils (Supplementary Fig. S1).

4.2.2. Lake Alchichica microbialites. The white and brown Alchichica microbialite samples contained 17 and 89 wt % aragonite, respectively, with the remainder being hydromagnesite. Both samples had biofilms on their exteriors, seen as dark green areas (Fig. 4). Therefore, sample exteriors were avoided when examining these samples to focus on entombed or mineralized biomass within sample interiors as opposed to surficial biomass. Microbialite samples had iron staining, including in a thick band (~1 cm wide) in the white hydromagnesite-rich sample (Fig. 4A). The brown aragonite-rich sample (Fig. 4B) also had hollow, tube-like features on its exterior, which may have formed as casts of the encrusted stems of vascular water plants (Kaźmierczak *et al.*, 2011).

The Alchichica microbialites both contained entombed biomass, suggesting a greater potential for fossilization. The white hydromagnesite-rich microbialite had notably fewer biomorphic features than the brown aragonite-rich one. In both samples, morphological biosignatures were found exclusively in the aragonite with hydromagnesite lacking entombed biomass. The hmgs-rich microbialite sample contained numerous spherical structures, interpreted as fossilized cells that were ~4 μm in diameter and were exclusive to the aragonite sections (Fig. 4C). Electron microscopy of the brown microbialite showed an abundance of diatom frustules and organic spheres (diameter = 4 μm; Fig. 4D), interpreted as coccoid cells, within aragonite, that were most easily observed in the acid-etched samples.

The spherical structures in the aragonite of the white microbialites were also visible under SEM (Fig. 4E, F), with the presence of iron coatings being confirmed by EDS. Coccoid, N_2-fixing cyanobacteria are a common feature of Alchichica microbialites, and their iron oxide coatings could be related to nitrogenase activity (Falcón *et al.,* 2020). The arg-rich microbialite also contained organic tubes, interpreted as well-preserved filamentous cyanobacteria (Fig. 4G). The Supplementary Information includes additional micrographs showing the iron-coated spheres and organic tube and filament structures (Supplementary Fig. S2).

4.2.3. Qinghai-Tibet Plateau samples. The Dujiali Lake hydromagnesite sediments were bright white, lightly consolidated, but not lithified (Fig. 5A). There are no substantial biofilms or microbial mats along the lake's margins where

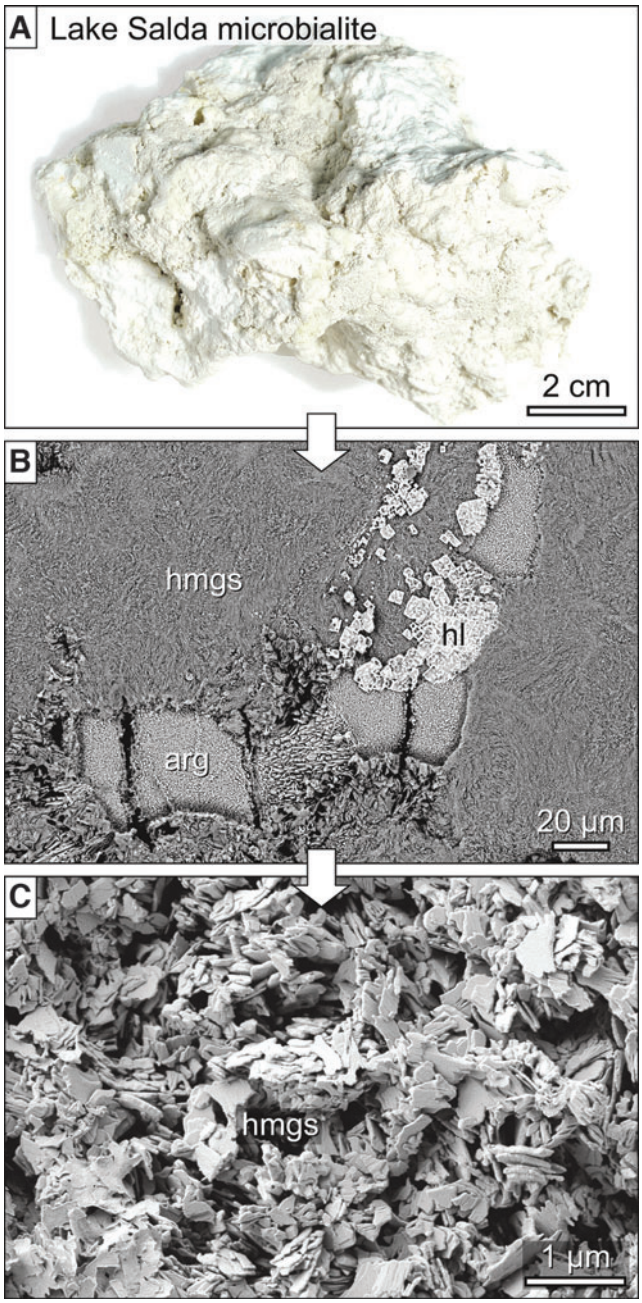

FIG. 3. Photograph of the hydromagnesite-rich stromatolite from Lake Salda, Turkey **(A)**. **(B)** Representative electron micrograph of a polished sample showing hydromagnesite (hmgs) and aragonite (arg) lacking any entombed biomass or morphological biosignatures. The presence of halite (hl) suggests that this sample formed under subaerial evaporative conditions. **(C)** An acid-etched sample showing the platy crystal morphology of hydromagnesite (hmgs) and the absence of entombed biomass. Color images are available online.

the sample was collected (Fig. 1D). Similarly, there were no biofilms associated with the Qaidam Basin aragonite ooids that were found along a palaeo-shoreline with no associated water. These ooids are ~200–600 μm and are nearly spherical with peloid nuclei. Concentric laminations were visible when thin sections were viewed using light microscopy (Fig. 5B). The hydromagnesite in the sediments had a platy crystal morphology and was highly porous (Fig. 5C). There was no visible evidence of entombed biomass or microfossils. The ooids were not lithified together to form an oolite; however, the individual ooids were hard and not easily broken. Although acid etching revealed the aragonite crystals' elongated morphology, there was no evidence of microbes among the eight ooids examined with SEM (Fig. 5D). Additional micrographs of the hydromagnesite sediments and acid-etched ooids are available in Supplementary Fig. S3.

4.2.4. Atlin playa samples. The Mg-carbonate sediments at the surface of the playa have previously been studied extensively (Power *et al.,* 2009, 2014, 2019). These white sediments are not consolidated or lithified and contain very low abundances of organic matter. Although filamentous cyanobacteria are occasionally found on these sediments (Fig. 6A), there is no abundant microbial biomass in the form of biofilms or microbial mats. These unconsolidated sediments are composed of mixtures of platy hydromagnesite and blocky magnesite crystals (Fig. 6B) that lack entombed biomass.

The Atlin microbialite contained clear macroscopic biosignatures, having an alveolar-septal structure that resembles some of the living microbial mats that have been documented at the site (Fig. 6C). The pisolite comprised mm-scale pisoids with inverse-graded bedding (Fig. 6D). Both samples had iron staining, but aragonite was the only mineral phase detectable when using XRD. Light microscopy of the microbialite revealed numerous tube structures (10–15 μm wide; 100s micrometer long), interpreted as fossilized filamentous cyanobacteria or algae (Fig. 6E). This sample also contained abundant pennate diatom frustules and some spherical structures resembling coccoid cells, which were identified with SEM. The pisolite also contained diatom frustules, yet fewer organic filaments resembling filamentous bacteria than the microbialite (Fig. 6F). The biosignatures in the pisolite were predominately concentrated near the center of each pisoid.

The Atlin samples contained ample evidence of biologic preservation within the matrix of aragonite needles that was readily observed in polished and acid-etched samples using SEM. Biogenic morphologies that were observed included deflated cells, diatom frustules, amorphous organics resembling extracellular polymeric substances, and filamentous structures interpreted as cyanobacteria (Fig. 6G, H). Spherical structures and diatoms were more abundant in the microbialite than the pisolite, which is consistent with petrographic examinations. These organic structures are reminiscent of the numerous filamentous and coccoid microbes that have been observed within microbial mats in the Atlin playa ponds (Power *et al.,* 2007; McCutcheon *et al.,* 2014, 2019). The Supplementary Information includes additional light and electron micrographs of diatom frustules and organic filaments and spheres that are interpreted as microbial remnants (Supplementary Fig. S4).

4.2.5. Clinton Creek mine samples. The Mg-carbonate efflorescences are bright white and cement the chrysotile tailings at the mine (Fig. 7A), whereas the aragonite microbialites have formed in the open pit pond (Fig. 7B). The efflorescences are a mix of nesquehonite, dypingite, and

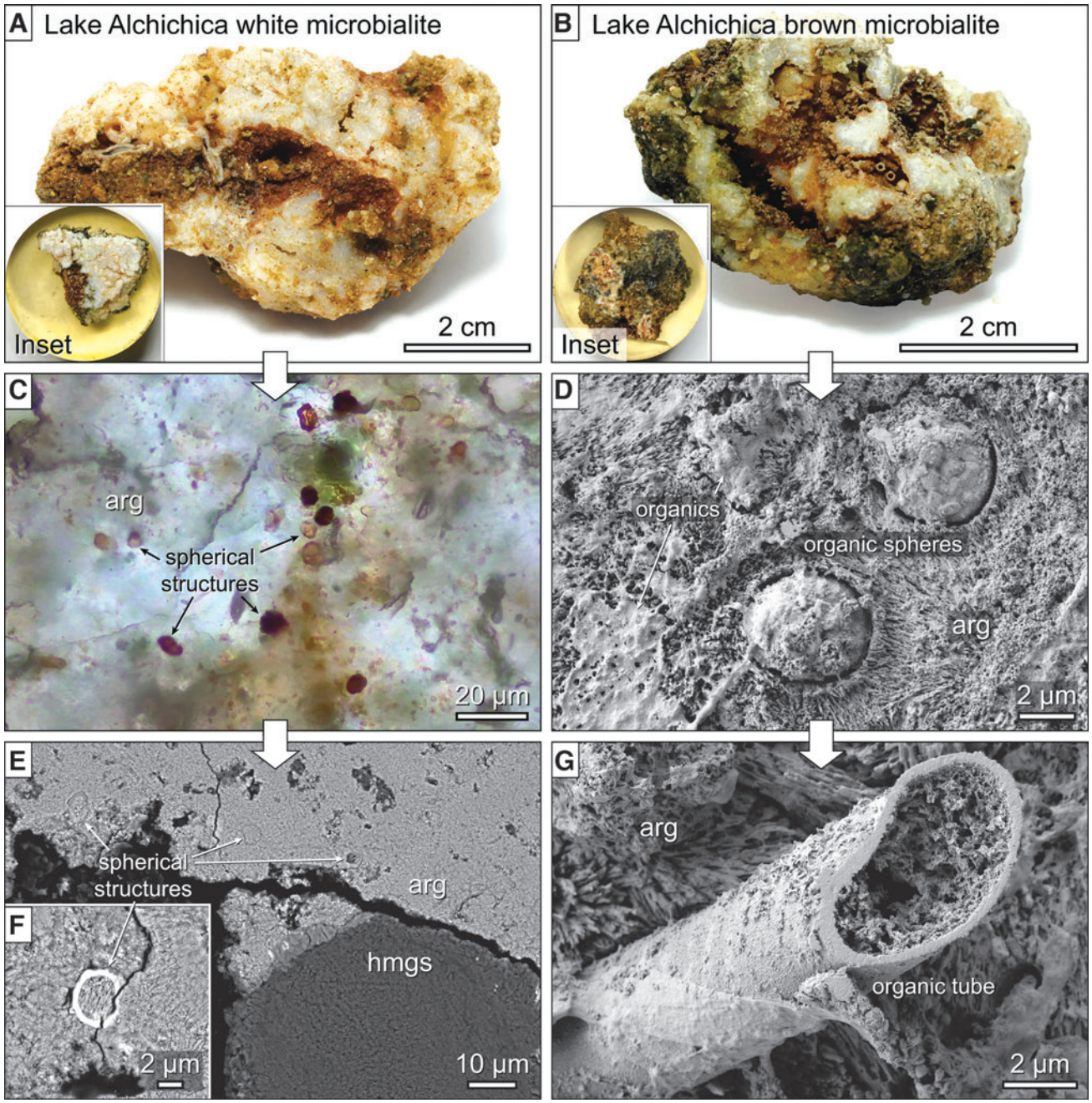

FIG. 4. Photographs of the **(A)** white hydromagnesite-rich and **(B)** brown aragonite-rich microbialites from Lake Alchichica, Mexico. The insets are photographs of the embedded and polished samples (mould diameter = 25 mm) to show the difference in coloration: white being hydromagnesite and brown being aragonite. **(C)** Spherical structures, interpreted as microbial cells, displaying iron oxide coatings and found within the aragonite of the white microbialite sample. **(D)** Well-preserved spherical structures, interpreted as microbial cells, exposed after acid etching within aragonite of the brown microbialite. **(E)** Hydromagnesite devoid of entombed biomass or microfossils within the white microbialite. Note the sharp boundary between the hydromagnesite (hmgs) and aragonite (arg). The aragonite contained numerous spherical structures, interpreted as mineralized coccoid cells (diameter $\approx$ 4 µm), that appeared bright using a backscatter electron detector, and the EDS confirmed the presence of iron **(F)**. **(G)** The brown microbialite contained a greater abundance of aragonite with entombed biomass, including organic filaments resembling filamentous cyanobacteria. EDS = energy dispersive spectrometer. Color images are available online.

hydromagnesite (Fig. 7C), which is consistent with previous mineralogical assessments (Wilson *et al.,* 2009). The Clinton Creek microbialite had a clotted texture with no laminations and contained detritus, including quartz and serpentinite grains, and fibrous chrysotile, consistent with XRD analysis. Thin sections revealed an abundance of diatom frustules and filamentous structures resembling cyanobacteria or algae within the layers of micritic aragonite (Fig. 7D). The aragonite needles fanned out to form spherulites that were best seen under cross-polarized light. Aragonite fluoresces blue under UV light, while entombed biomass near spherulite centers fluoresced pink/red due to

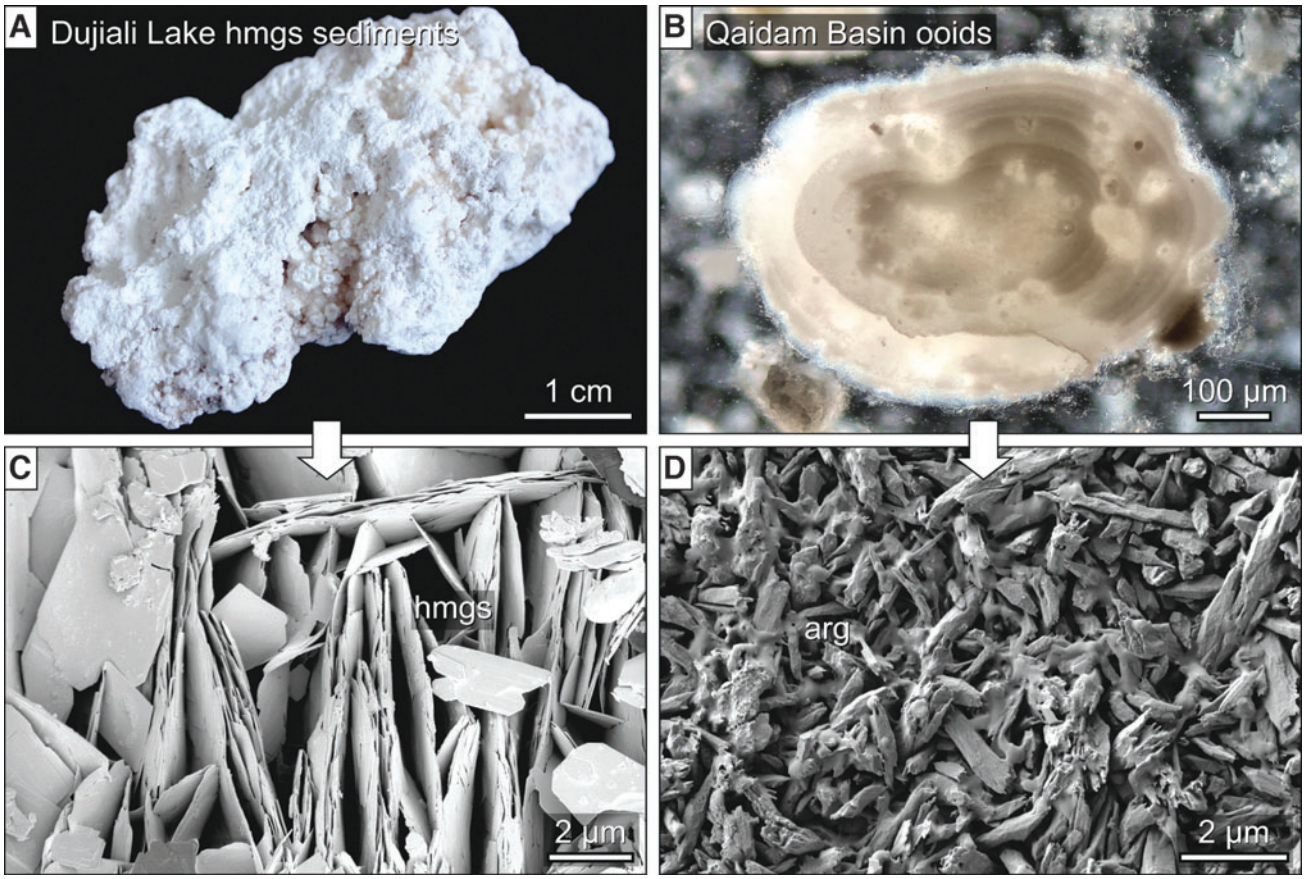

FIG. 5. Samples from the Qinghai-Tibetan Plateau, China. **(A)** A hand specimen of hydromagnesite sediments from Dujiali Lake and **(B)** a thin section micrograph of an aragonite ooid from Qaidam Basin. **(C)** The hydromagnesite at Dujiali Lake has a platy crystal morphology, and sediments are lightly cemented but not lithified. **(D)** An acid-etched ooid showing the elongated crystal morphology of aragonite. Neither sample contained identifiable entombed biomass or microfossils. Color images are available online.

the presence of chlorophyll (Supplementary Fig. S5D, E) (Power *et al.,* 2011).

The Clinton Creek microbialite contained the highest proportion of diatoms from all five field sites. Amorphous organics that resembled extracellular polymeric substances and organic tubes, interpreted as filamentous cyanobacteria, were also present in acid-etched samples when viewed with SEM. In comparison, the Mg-carbonate efflorescences lacked entombed biomass (Fig. 7E), whereas acid-etched and preserved samples of the aragonite microbialites contained an abundance of microbial remnants, including filamentous cyanobacteria (Fig. 7F). Additional light and electron micrographs of the Mg-carbonate efflorescences and microbialite are available in Supplementary Fig. S5.

5. Discussion

For the five analog sites, we considered the environmental and mineralogical controls on entombing biomass with the potential for preserving morphological biosignatures (Fig. 8). Regarding the environment, we considered smaller subenvironments rather than the larger scale environment, for example, ponds within the Atlin playas. Although microbes are ubiquitous in Earth's surface environments, including the five terrestrial analogs, biofilms and microbial mats are not prevalent. Therefore, the likelihood of biosignature preservation is considerably greater where microbial biomass is abundant, that is, there are more microbes to potentially entomb and preserve (vertical axis in Fig. 8).

FIG. 6. Photograph of unconsolidated sediments from the Atlin hydromagnesite–magnesite playas (British Columbia, Canada) colonized by filamentous cyanobacteria **(A)**. Electron micrograph of the sediments showing the platy and blocky (rhombohedral) crystal morphologies of hydromagnesite and magnesite, respectively. Photographs of the aragonite microbialite **(C)** and pisolite **(D)** from the playas. Note the inverse graded bedding of the pisolite is from left (finer) to the right (coarser) in this photograph. **(E)** Thin section micrograph of the microbialite showing numerous diatom frustules and filamentous structures, interpreted as mineralized cyanobacteria (see inset). **(F)** Thin section micrograph of the pisolite showing some diatom frustules and filaments. Both samples contained organic filaments that were best observed in acid-etched samples **(G, H)**. Color images are available online.

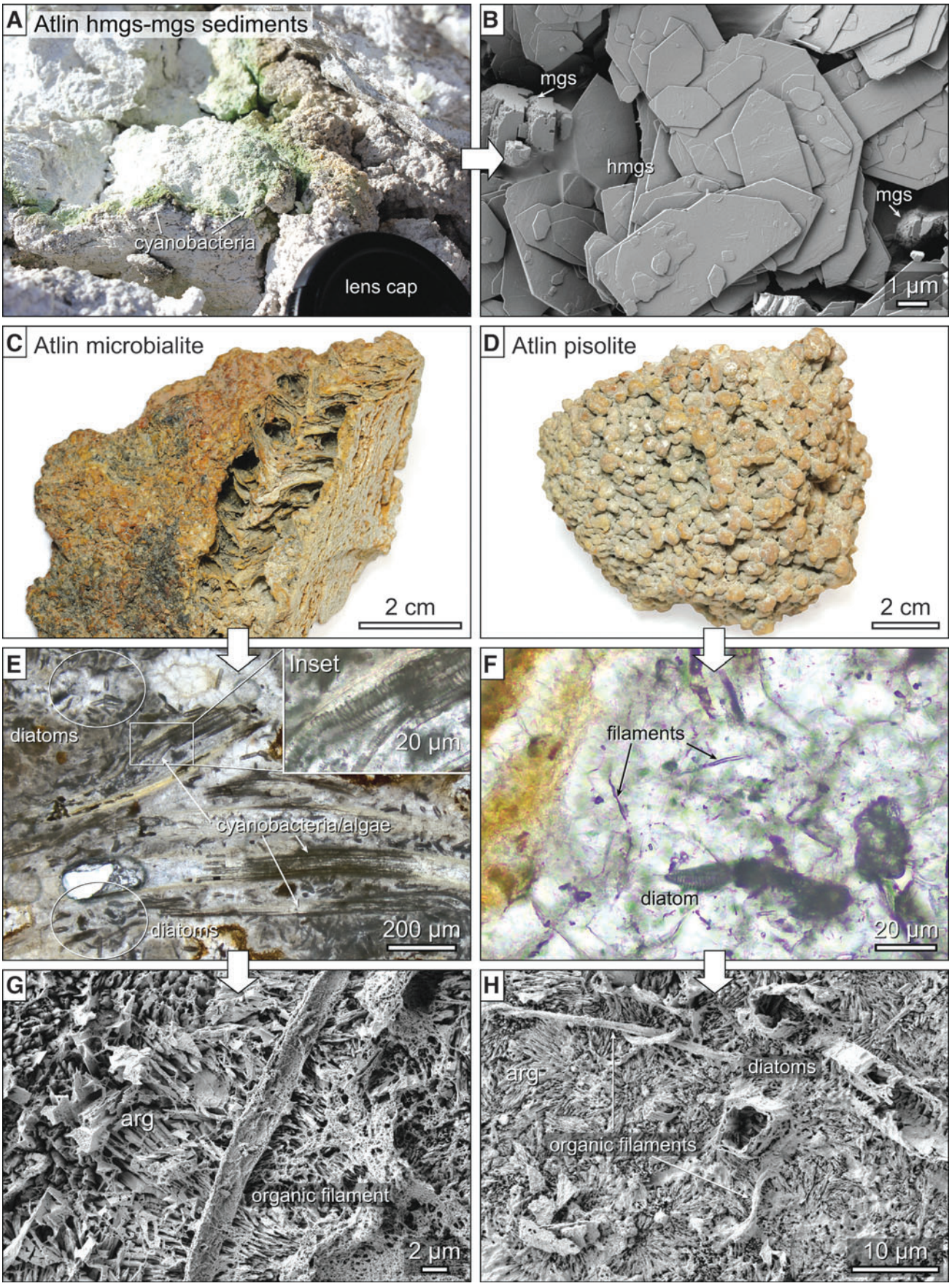

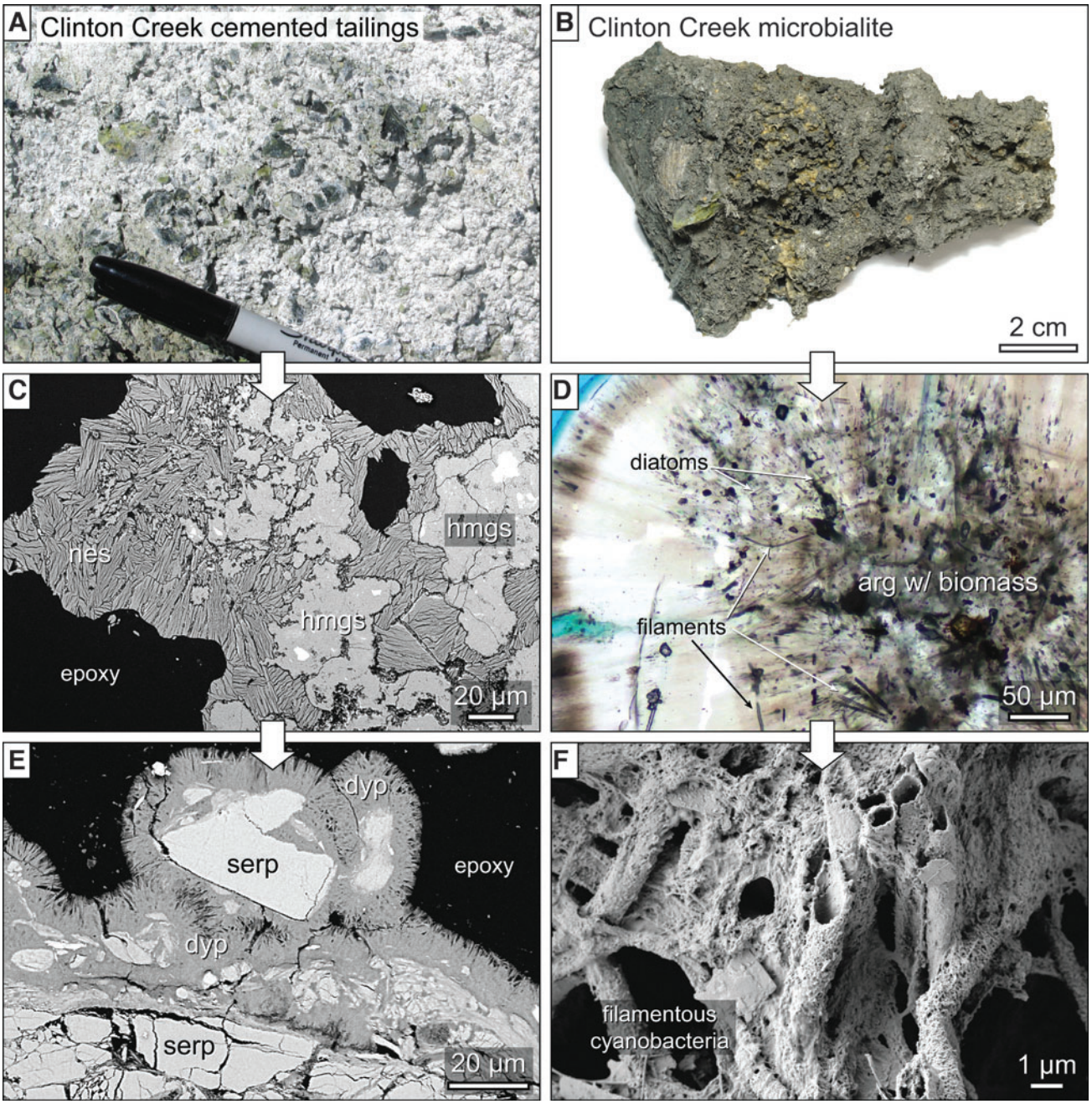

FIG. 7. A field photograph of the Clinton Creek chrysotile mine tailings cemented by hydrated Mg-carbonate efflorescences (marker for scale; **A**). Photograph of an aragonite microbialite specimen collected from the open pit pond (**B**). These two environments are contrasted by the mode of formation: subaerial *in situ* precipitation of Mg-carbonates, including hydromagnesite (hmgs), dypingite (dyp), and nesquehonite (nes; **C**) versus subaqueous aragonite precipitation in the open pit pond (**D**). The aragonite microbialites contain an abundance of diatom frustules and cyanobacteria (**D**). The mineralogical composition of the efflorescences indicates that mineral transformations are occurring, for example, nes → dyp → hmgs (**C, E**). Acid-etched and preserved samples of microbialite contained an abundance of entombed biomass, including filamentous organic structures interpreted as cyanobacteria (**F**). Color images are available online.

From a mineralogical perspective, a mineral that is suitable for preserving biosignatures will: (1) form fast or at a rate similar to microbial growth, (2) be stable for long periods, (3) form in an environment where microbes thrive, and (4) tend to lithify to form rock (Table 3). These mineral properties will increase the likelihood of biomass entombment and, ideally, biosignature preservation (horizontal axis in Fig. 8).

5.1. Environmental controls on biosignature preservation

The water chemistry of a given site mainly depends on the geological and hydrological setting. For the analog sites, Mg-rich waters are often a result of the weathering of mafic and ultramafic bedrock and evapoconcentration (Table 1). From these waters, authigenic carbonate minerals may

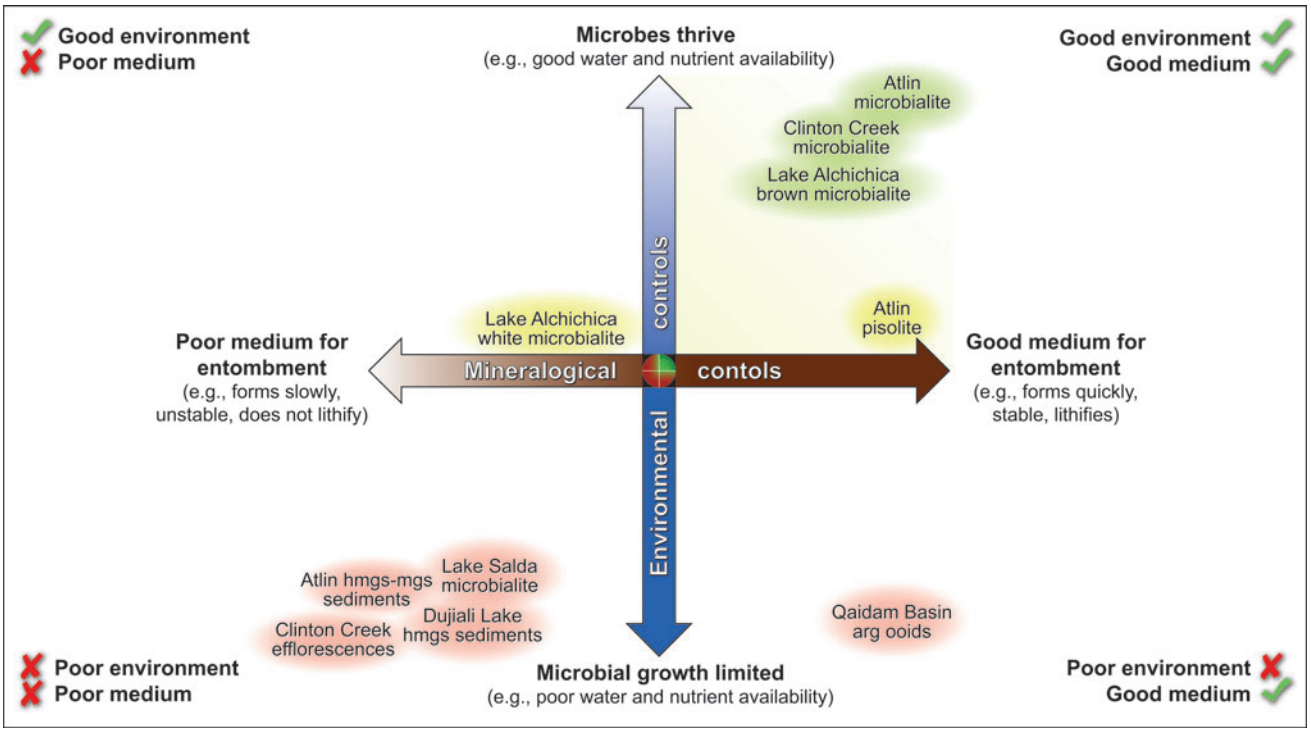

FIG. 8. A quadrant diagram illustrating the environmental (vertical axis) and mineralogical (horizontal axis) controls for entombing microbial biomass in environments with authigenic mineral deposition. The ideal environment (top half) accumulates water and nutrients for microbes to thrive. The ideal mineral medium (right half) forms quickly or at a rate similar to microbial growth, is stable (*i.e.,* will not transform), and tends to lithify. The relative positions of the samples studied from the five analog sites are plotted (Table 2). Samples dominated by aragonite and that formed in subaqueous environments plot in the top-right quadrant and had an abundance of entombed biomass. Color images are available online.

precipitate and entomb microbial biomass with the potential for biosignature preservation. These minerals include those identified in the samples: magnesite (Atlin only), hydromagnesite (most common), dypingite and nesquehonite (Clinton Creek only), and aragonite (Table 2). Some site waters are saturated with respect to these minerals, while others are undersaturated relative to carbonate minerals that are present at the site and, thus, would require mediation, such as evaporation or a biological process to induce precipitation. Alternatively, waters may have been saturated with respect to these minerals in the past; however, it is not within the scope of this study to make those determinations.

Table 3. Mineral Abundances at Sites and Ideal Properties for Biosignature Preservation

	Mgs	*Hmgs*	*Dyp*	*Nes*	*Arg*
Analog site					
Lake Salda stromatolites/tufa		M			m
Lake Alchichica microbialites		M			M w/biomass
Dujiali Lake sediments		M			m
Qaidam Basin ooids					M
Atlin Mg-carbonate sediments	M	M			
Atlin microbialites/pisolite					M w/biomass
Clinton Creek efflorescences		M	M	M	
Clinton Creek microbialites					M w/biomass
Ideal mineral properties for entombing biomass					
Fast precipitation rates			✓	✓	✓
Relatively stable	✓	✓			✓
Lithifies					✓
Tends to form subaqueously where microbes may thrive			✓		✓
Abundant in environment		✓			

Carbonate minerals found at the analog sites include magnesite (mgs), hydromagnesite (hmgs), dypingite (dyp), nesquehonite (nes), and aragonite (arg). The abundances in the samples are listed as either major (M; >10 wt %) or minor (m; <10 wt %). Minerals containing substantial entombed biomass are labeled (w/biomass). The second half of this table lists the ideal mineral properties for entombing microbial biomass.

The hydrated Mg-carbonate minerals (*e.g.,* hydromagnesite) are more likely to form under highly evaporative conditions that increase the concentrations of Mg and dissolved inorganic carbon. Although the Lake Salda waters are supersaturated with respect to hydromagnesite and aragonite, Mg-carbonate formation in Lake Salda relies on microbial processes. Observations and laboratory experiments by Balci *et al.* (2020) found that evaporation alone does not trigger the precipitation of hydromagnesite. Furthermore, laboratory experiments for which cyanobacteria and Lake Salda water were used resulted in dypingite, not hydromagnesite, precipitation (Shirokova *et al.,* 2013). Thus, hydromagnesite does not precipitate directly from lake water, yet it is the main mineral in the stromatolites.

Lake Alchichica waters are saturated relative to hydromagnesite and aragonite, which are both found in the microbialites. Sharp boundaries separated these two minerals in the microbialites (Fig. 4E), indicating that there may have been significant shifts in the environmental conditions within the lake or locally within the microbialites. For instance, Zeyen *et al.* (2021) have suggested that the composition of these microbialites is controlled by shifts between subaqueous and subaerial carbonate depositions due to changes in lake level or temporal variations in lake chemistry, that is, Ca concentrations. These shifts could significantly affect carbonate mineralogy and, thus, the entombment of microbes.

The Dujiali Lake water is undersaturated with respect to hydromagnesite and must be evaporated by at least 65% to reach saturation. Furthermore, these waters would need to be evaporated by 75% and 90% to become saturated in dypingite and nesquehonite. Although the Clinton Creek tailings water is saturated with respect to hydromagnesite, it is undersaturated with respect to dypingite and nesquehonite, which are both found in the Mg-carbonate efflorescences (Wilson *et al.,* 2009). These waters would need to be evaporated by 40% and 95% to become saturated with respect to dypingite and nesquehonite, respectively. Thus, highly evaporative conditions are required to produce the observed mineral assemblages, which exist in subaerial settings such as playas, exposed sediments, and lake margins.

Subaerial settings are generally less conducive for biomass accumulation than ponds and lakes that contain water and accumulate nutrients. Even subaerial phototrophic biofilms are recognized to be more prosperous under conditions of higher water content to promote nutrient distribution (Vázquez-Nion *et al.,* 2018). The unfavorable environment for microbial growth in subaerial settings may explain the lack of microbial remnants observed in the hydromagnesite-rich samples from the terrestrial analog sites. For example, halite identified in the Lake Salda samples (Fig. 3) strongly indicates subaerial formation, and significant microbial remnants were not found in this sample. Furthermore, cyanobacterial remains within the hydromagnesite of Lake Alchichica are rare (Kaźmierczak *et al.,* 2011).

Although subaerial conditions are favorable for hydromagnesite precipitation, these settings are water- and nutrient-poor with limited microbial growth. For instance, the filamentous cyanobacteria on some Atlin hydromagnesite sediments (Fig. 6A) have heterocysts for fixing nitrogen (Power *et al.,* 2007). Yet, their growth is likely limited by phosphorous availability.

The microbialites from Alchichica, Atlin, and Clinton Creek contained an abundance of entombed biomass, which was found exclusively in aragonite. These microbial remnants included diatom frustules, organic structures interpreted as coccoid and filamentous cells, and amorphous organics, possibly extracellular polymeric substances. The waters of Lake Alchichica, Atlin playa ponds, and the open pit pond at Clinton Creek are all saturated with respect to calcite, aragonite, and magnesite (Table 1). However, of these minerals, only aragonite was detected in the samples; thus, the SIs are a good predictor of aragonite formation, which is not the case for calcite and magnesite. The formation of aragonite is thermodynamically controlled, meaning it will precipitate if waters are saturated (*e.g.,* favorable [Ca], pH, and dissolved inorganic carbon) (Jones, 2017).

The precipitation of aragonite instead of its polymorph, calcite, at the field sites occurs because the $[Mg^{2+}]/[Ca^{2+}]$ molar ratios are >2, thus inhibiting calcite formation (Table 2) (Aquilano *et al.,* 2020). The aragonite in the Alchichica, Atlin, and Clinton Creek samples appears to have formed subaqueously (Kaźmierczak *et al.,* 2011; Power *et al.,* 2011) or at the very least under fluctuating water levels (Bolton *et al.,* 1988; Power *et al.,* 2009). These environments provide better water availability and are more nutrient-rich, making them favorable for microbial growth and biomass accumulation. Therefore, the tendency of aragonite to precipitate subaqueously improves the likelihood of entombing microbes within the microbial mat itself (Couradeau *et al.,* 2013) or following the colonization of mineral surfaces (Power *et al.,* 2011).

The stable carbon and oxygen isotope data provide further insight into the environmental conditions under which the carbonate minerals formed. Because of the diverse environmental conditions of the five terrestrial analogs, it is more informative to compare the aragonite- and hydromagnesite-rich samples from a single site (Fig. 2; *e.g.,* Alchichica, Atlin, Clinton Creek). The isotopic differences between the stable carbon ($\Delta^{13}C_{hmgs\text{-}arg} = 1.1‰$ VPDB) and oxygen ($\Delta^{18}O_{hmgs\text{-}arg} = 2.5‰$ VSMOW) equilibrium fractionation factors of hydromagnesite (O'Neil and Barnes, 1971; Mook *et al.,* 1974; Wilson *et al.,* 2010) and aragonite relative to CO_2 and water, respectively (Tarutani *et al.,* 1969; Romanek *et al.,* 1992), at 25°C, cannot account for the measured enrichments in ^{13}C and ^{18}O seen in the hydromagnesite-rich samples compared with the aragonite-rich samples from the same sites (Fig. 2).

For example, hydromagnesite and aragonite are spatially distinct at the submillimeter scale within the Lake Alchichica microbialites (Fig. 4), suggesting that they may have formed at different times and under different conditions. The Alchichica white (hmgs-rich) microbialite had $\delta^{13}C$ and $\delta^{18}O$ values that were +3.9‰ and +6.5‰ greater than the brown (arg-rich) microbialite. Again, these differences cannot be explained by the equilibrium fractionation of stable C and O isotopes from the same water, which implies that these minerals may have formed from different waters that were isotopically distinct. For instance, the hmgs-rich microbialite may have formed under more subaerial evaporative conditions, enriching ^{13}C and ^{18}O due to CO_2 degassing and evaporation (Power *et al.,* 2014).

The Atlin hydromagnesite–magnesite surface sediments and Clinton Creek Mg-carbonate efflorescences are known

to have formed under subaerial evaporative conditions based on field observations. These samples were also enriched in ^{13}C and ^{18}O compared with aragonite samples from the same sites (Fig. 2).

The Clinton Creek mine is an informative example of how environmental conditions influence carbonate precipitation and microbial growth. The two subenvironments, the open pit pond and tailings pile, differ significantly in the modes of carbonate formation and resulting mineralogy (Wilson *et al.,* 2009; Power *et al.,* 2011; White *et al.,* 2015). The open pit pond accumulates water and nutrients for microbes to thrive, resulting in periphyton and biofilms on rock surfaces in waters where aragonite precipitates to entomb microbes. These waters are undersaturated with respect to hydromagnesite and favor aragonite over calcite precipitation due to the high $[Mg^{2+}]/[Ca^{2+}]$ ratio. In contrast, the subaerial tailings lack abundant microbial growth due to lower water availability and insufficient nutrients. These tailings, a natural analog for ultramafic tephra, are composed almost entirely of serpentine with only trace essential nutrients (Wilson *et al.,* 2009). Consequently, the Mg-carbonate efflorescences lacked recognizable microbial remnants or identifiable microfossils.

The aragonite within the Lake Salda microbialites and the aragonite ooids from Qaidam Basin lacked microbial remnants. It is possible that the aragonite in the former sample was mainly precipitated in subaerial conditions that lacked abundant biomass, or there may be other samples that do contain microfossils within aragonite, which requires further investigation. Although the Qaidam Basin ooids likely formed subaqueously, it is impossible to determine whether they were associated with microbial mats or biofilms, given that the lake no longer exists (Lin *et al.,* 2022).

5.2. Mineralogical controls on biosignature preservation

In some samples, including the Atlin and Dujiali hydromagnesite sediments and Clinton Creek efflorescences, the absence of entombed biomass can mainly be explained by a lack of pervasive microbial communities in the form of biofilms and microbial mats. However, substantial microbial populations associated with the hydromagnesite stromatolites from Lake Salda have been well documented (Braithwaite and Zedef, 1996; Russell *et al.,* 1999; Balci *et al.,* 2020). This observation suggests that in addition to substantial microbial populations and authigenic mineral formation, there are mineralogical controls on biomass entombment (Table 3). The carbonate minerals present at the natural analogs that may entomb biomass, potentially leading to biosignature preservation, include magnesite, hydromagnesite, dypingite, nesquehonite, and aragonite. The properties of these minerals, including (1) formation rate, (2) stability, and (3) ability to lithify, will affect the entombment of microbial biomass and, thus, biosignature preservation potential.

5.2.1. Mineral formation rates. For biosignatures to be preserved in the geological record, the formation rate of distinctive biological features must be greater than the rate of destruction from various processes, including weathering and diagenesis (Hays *et al.,* 2017). Similarly, better biosignature preservation may be associated with faster mineral precipitation rates, that is, the rate of biomass entombment is greater than the biomass degradation rate. In this study, we considered the precipitation rates of magnesite, hydrated Mg-carbonate minerals, and aragonite.

Magnesite is the stable form of Mg-carbonate; however, it was only detected at one of the analog sites, the Atlin playa sediments. Furthermore, its formation rate is exceedingly slow at Earth's surface conditions due to the strong hydration of Mg^{2+} ions (Saldi *et al.,* 2009, 2012; Power *et al.,* 2019). For example, the rate of magnesite formation in the Atlin playas ranges from 10^{-17} to 10^{-16} mol/(cm$^2\cdot$s) (Power *et al.,* 2019). Thus, forming a detectable amount of magnesite ($\sim$1 wt % by XRD) requires 100s–1000s of years (Power *et al.,* 2019). These rates are likely too slow to encapsulate microbes during magnesite formation, making this mineral an unlikely candidate for preserving biosignatures.

Hydromagnesite is the most abundant carbonate mineral at the analog sites as it is stable for 1000s of years (Power *et al.,* 2014; Lin *et al.,* 2017). If it were a good medium for biosignature preservation, its high abundance would increase the likelihood of finding and observing biosignatures. However, hydromagnesite precipitation is also typically kinetically controlled at temperatures <40°C, whereas magnesite precipitation is kinetically controlled at <60°C (Königsberger *et al.,* 1999; Hänchen *et al.,* 2008; Gautier *et al.,* 2014). Furthermore, there has not been an experimental study demonstrating direct nucleation and precipitation of hydromagnesite at Earth's surface temperatures from an aqueous solution that is free of any solids, but rather numerous studies show that it forms from precursor minerals such as nesquehonite and dypingite (Davies and Bubela, 1973; Hopkinson *et al.,* 2012).

Consequently, the direct precipitation of hydromagnesite and magnesite at the field sites is likely slow. Organic molecules and structures often degrade rapidly due to heterotrophic respiration and oxidation in aerobic environments, implying that faster mineral formation results in better preservation (Li *et al.,* 2013). The slow precipitation rates of hydromagnesite may also make it a poor medium for biosignature preservation.

SIs for aragonite and hydromagnesite of the site waters were good predictors of whether these minerals would be present in the samples (Table 1). For example, the Atlin ponds and the Clinton Creek open pit pond were undersaturated with respect to hydromagnesite, and samples from these subenvironments did not contain hydromagnesite. Conversely, hydromagnesite was saturated in waters from sites where hydromagnesite samples were collected (*e.g.,* Lake Salda), implying that this mineral precipitated directly from the waters despite its precipitation being kinetically controlled.

However, studies of the Atlin playas and Clinton Creek tailings concluded that hydromagnesite often forms via transformation from more hydrated phases (Wilson *et al.,* 2009; Power *et al.,* 2014, 2019). Dypingite, nesquehonite, and lansfordite are known to precipitate rapidly when waters are saturated, that is, their precipitation is not kinetically controlled (Ming and Franklin, 1985; Kloprogge *et al.,* 2003; Power *et al.,* 2007; Wilson *et al.,* 2010; Harrison *et al.,* 2019). Dypingite is saturated in Lake Salda (as is nesquehonite) and Lake Alchichica and may be a likely

precipitate, although it was not detected with XRD in samples from either site. Atlin pore waters are saturated with respect to lansfordite, which is found at the water table. Hydrated Mg-carbonate minerals are all undersaturated in Dujiali Lake waters and the Clinton Creek tailing pore waters and would require significant evapoconcentration to induce precipitation. While the slow precipitation rates of magnesite and hydromagnesite are likely to hinder biomass entombment, aragonite forms relatively rapidly, which may partly explain the greater abundance of microbial biomass seen in the arg-rich samples.

5.2.2. Mineral stability. Given that hydromagnesite precipitation is kinetically controlled, its occurrence at the field sites may indicate its formation through the transformation of metastable precursors. Lansfordite, nesquehonite, and dypingite are known to rapidly dehydrate and transform into hydromagnesite, which is stable for 1000s of years at Earth's surface conditions (Davies and Bubela, 1973; Hamilton *et al.,* 2016; Power *et al.,* 2016; Harrison *et al.,* 2019, 2021). These transformations may be the dominant pathway for forming hydromagnesite at the terrestrial analog sites as opposed to direct precipitation from waters. Transformations among hydrated Mg-carbonate minerals occur through a series of coupled dissolution–precipitation reactions, meaning that one phase (*e.g.,* nesquehonite) dissolves in water films or pore waters where a less hydrated phase (*e.g.,* dypingite) precipitates. The reactions proceed from the most hydrated to the least hydrated magnesium carbonate species; occasionally, lansfordite [$MgCO_3 \cdot 5H_2O$] forms first, often forming at <10°C, followed by nesquehonite, dypingite, and hydromagnesite.

Previous studies of the Atlin playas showed that the main pathway for magnesite formation was direct precipitation from pore fluids and not the transformation of hydromagnesite (Power *et al.,* 2019; Mavromatis *et al.,* 2021).

Mineral transformations and changes in crystal morphology may be detrimental to preserving entombed biomass and biosignatures. The transformation of hydrated Mg-carbonates through coupled dissolution–precipitation reactions induces changes in the mineral volume and morphology. Material can be lost in the fluid phase when more solid volume is dissolved than reprecipitated, resulting in increased porosity with each transformation (Ruiz-Agudo *et al.,* 2014). The porosity of hydrated Mg-carbonate minerals may increase as minerals with prismatic morphologies (lansfordite and nesquehonite) are transformed into minerals with a flakey (dypingite) or platy (hydromagnesite) morphology. These transformations may expose entombed biologic features to fluids that might hinder biosignature preservation by enabling microbial decomposition or exposure to radiation.

This concept of entombment into a matrix of lower porosity crystals is exemplified in micritic aragonite. Spherulites that comprised micritic aragonite were observed in samples from Atlin, Clinton Creek, and Lake Alchichica. These spherulites incorporated microbial biomass such as filaments, cells, and diatoms within the needle-like aragonite crystals radiating to form the spherulite. On the contrary, hydromagnesite did not contain microbial biomass within its more porous and platy morphology.

Aragonite is known to transform into the thermodynamically stable $CaCO_3$ polymorph calcite within metamorphic contexts under the mediation of a solvent or by heat in a solid-state transformation (Koga *et al.,* 2013; Koga and Nishikawa, 2014). However, it is unclear to what extent aragonite will transform under Earth's surface conditions without higher temperatures and pressures or reacting fluids. Furthermore, it is unknown whether biosignatures would be destroyed during the aragonite-to-calcite transition. Further studies and experimentation are needed to address these uncertainties.

5.2.3. Ability to lithify sediments. Aragonite's acicular habit and relatively higher hardness (Mohs hardness = 3.5–4) and density (2.93 g/cm^3) contribute to strong cementation (Xu *et al.,* 2021). The interlocking of aragonite needles seen in the Lake Alchichica microbialites (Fig. 4D, G), Qaidam Basin ooids (Fig. 5D), Atlin microbialite (Fig. 6G) and pisolite (Fig. 6H), and Clinton Creek microbialites facilitates the lithification of these samples (Haredy *et al.,* 2019). Hydromagnesite has a lower hardness (3.5), density (2.18 g/cm^3), and a platy crystal habit that does not interlock. Aragonite needles were typically 10s of micrometers in length, whereas hydromagnesite plates were typically no >5 μm wide and <1 μm thick. This difference in size may also contribute to aragonite being able to lithify more easily than hydromagnesite.

Although magnesium carbonates may cement materials (Power *et al.,* 2021), this should be considered different from the lithification process that forms rock. The Atlin playas best illustrate the contrast in lithification potential between hydromagnesite and aragonite. The aragonite microbialite and pisolite were found among piles of rubble (Fig. 1G) and were lithified as hand specimen-sized rock samples that required a rock saw to cut. In contrast, the Atlin hydromagnesite sediments (Fig. 1G) are clay-like and are not even mildly consolidated such as the hydromagnesite microbialites at Lake Salda and Lake Alchichica, which can still be broken by hand. Fast lithification of carbonate minerals facilitates entombment of any associated biomass, likely leading to better biosignature preservation, and again, aragonite appears to have this advantage over hydromagnesite.

5.3. Implications for the search for biosignatures at Jezero Crater

Orbiter data were used to identify Mg-carbonates in the marginal carbonates at Jezero Crater (Ehlmann *et al.,* 2008; Horgan *et al.,* 2020). On Earth, authigenic magnesium carbonates form in various environments, including lakes, playas, caves, and marine settings (Scheller *et al.,* 2021). The marginal carbonates or other carbonate minerals at Jezero Crater may be relicts of a paleolacustrine environment. In that case, they could resemble the subaqueous or littoral deposits at Lake Salda, Lake Alchichica, Dujiali Lake, or Qaidam Basin. The Jezero carbonates may also have formed through the discharge and evaporation of Mg-HCO_3 waters and, therefore, could resemble the Atlin playas or a spring system (Knuth and Potter-McIntyre, 2021). Alternatively, weathering of ultramafic tephra may have resulted in the *in situ* deposition of Mg-carbonates. Thus, they may be similar to the Mg-carbonate efflorescences at the Clinton Creek mine.

Nevertheless, this study has shown that aragonite is often found in environments where Mg-carbonate deposition is

dominant. Therefore, it is plausible that aragonite could also be present at the Jezero Crater at a spatial resolution below orbiter detection limits (Hays *et al.,* 2017).

Previous studies have not identified aragonite on Mars (Fassett and Head, 2005; Ehlmann *et al.,* 2008; Horgan *et al.,* 2020; Mandon *et al.,* 2020); however, there is evidence of $CaCO_3$ formation (Niles *et al.,* 2013). Orbiter data of Leighton Crater, Mars, indicate spectra resembling calcite or siderite, as well as kaolinite-group minerals and hydrated Fe/Mg-bearing silicates (Michalski and Niles, 2010), similar to the minerals detected at Jezero Crater. In addition, early analysis of the nakhlite meteorites reported observations of carbonate veins composed of nearly pure $CaCO_3$ (Gooding *et al.,* 1991), which implies that aragonite could exist on Mars. Wray *et al.* (2016) identified Fe- and/or Ca-rich carbonates (*e.g.,* calcite, ankerite, and siderite) co-occurring with phyllosilicates by using CRISM data in and around the Huygens Basin northwest of Hellas, in western Noachis Terra.

Furthermore, Morris *et al.* (2010) identified magnesium–iron carbonate-rich rocks (16–34 wt %) in the Comanche outcrops at the Columbia Hills of Gusev Crater by way of the Mars Exploration Rover Spirit. The authors suggest that these carbonate outcrops imply extensive aqueous activity at circum-neutral pH conditions, which would be favorable for habitable environments on early Mars.

Jezero Crater is considered an ideal setting for biosignature preservation as a low-energy, long-lived, aqueous system with authigenic carbonate deposition where microbial calcification could occur (Vago *et al.,* 2019). The study of natural analogs provides invaluable insights into the environmental conditions and mineralogical controls that increase the likelihood of biosignature preservation. The challenge of identifying biosignatures at Jezero is to determine the probability of life producing a feature and the improbability of abiotic formation (Chan *et al.,* 2019; Knuth and Potter-McIntyre, 2021). Fortunately, as this study has argued, carbonate formation in subaqueous environments increases the probability of biotic formation because these settings accumulate water and nutrients for microbes to thrive, a stark contrast to subaerial settings. Regardless of whether aragonite is discovered on Mars, the present study highlights the importance of determining the environmental conditions and processes that drive the formation of authigenic carbonate minerals.

A better understanding of any carbonate minerals identified at the Jezero Crater that could be media for biosignature preservation will be essential. Magnesium carbonates, including magnesite and hydromagnesite, are not well suited to biosignature preservation; however, this should not exclude them from further investigation if identified in samples from Jezero Crater. The calcium carbonate mineral aragonite is a better medium for biosignature preservation based on the terrestrial analogs examined in this study; however, its presence, abundance, and stability over geological time under martian conditions remain open questions. Although not identified within any of the samples described in this study, calcite is likely just as good, if not better than aragonite, as a medium for biosignature preservation, given that calcite is the most stable form of $CaCO_3$. Hence, it would also be a valuable target for sample collection by Perseverance.

6. Conclusions

Mg-carbonate minerals, mainly hydromagnesite, are the dominant precipitates from alkaline, Mg-rich environments analogous to Jezero Crater. However, entombed microbial biomass and morphological biosignatures were absent within the Mg-carbonates at all five analog sites. This finding demonstrates that Mg-carbonates formed at Earth's surface conditions are a poor preservation medium for four reasons as follows:

(1) A tendency to form subaerially under evaporative environmental conditions that are not conducive for abundant microbial growth (*e.g.,* biofilms and mats).
(2) Slow formation rates (magnesite and hydromagnesite) that may prevent entombment of microbial biomass before it degrades.
(3) A tendency to transform (nesquehonite and dypingite) and possibly expose biosignatures to degradation.
(4) A tendency not to lithify, which eliminates entombment and promotes degradation of microbial biomass.

The present study of terrestrial analogs shows that aragonite is also present in all of these systems and, in many instances (Alchichica, Atlin, and Clinton Creek microbialites), contains abundant entombed microbial biomass. Subaqueous conditions, or conditions with high water availability, allow for abundant microbial growth. This greater biomass increases the likelihood of biosignature preservation. Aragonite may precipitate under these conditions without the need for high evapoconcentration, as is the case for the hydrated Mg-carbonate minerals. Furthermore, faster precipitation rates, greater stability compared with hydrated Mg-carbonates, and ease of lithification of aragonite make this mineral a preferred medium for biosignature preservation.

We have shown that aragonite is present within each of the five Mg-carbonate environments identified as potential analogs to Jezero Crater and that it contains entombed biomass with the potential to preserve biosignatures. The importance of aragonite and other calcium carbonates in these systems should not be overlooked when targeting rock formations for sample collection at Jezero Crater.

Acknowledgments

We want to thank Dr. Todd Simpson for his help with scanning electron microscopy at the Western Nanofabrication Facility at Western University. We are grateful to Dr. Chuanyong Ye and Dr. Wenxi Chen for their help in collecting hydromagnesite and ooid samples from the Qinghai-Tibetan Plateau. Thank you to the editor for handling our article and the two anonymous reviewers for their insightful and helpful comments that improved our article.

Authors' Contributions

T.M.B.: Investigation; visualization; and writing—original draft (lead). I.M.P.: Funding acquisition; conceptualization; project administration; supervision; visualization; and writing—review and editing (lead). C.P.: Formal analysis; investigation; and writing—review and editing. H.A.: Investigation and writing—review and editing. L.I.F.: Investigation and writing—review and editing. Y.L.: Investigation and writing—review and editing. S.A.W.: Investigation and writing—review and editing.

Author Disclosure Statement

No competing financial interests exist.

Funding Information

We acknowledge the support of the Natural Sciences and Engineering Research Council (NSERC) of Canada through a Discovery grant (RGPIN-2018-04490) and Tier 2 Canada Research Chair (CRC-2021-00338) to Power.

Supplementary Material

Supplementary Figure S1
Supplementary Figure S2
Supplementary Figure S3
Supplementary Figure S4
Supplementary Figure S5

References

Alleon J, Bernard S, Le Guillou C, *et al*. (2016) Early entombment within silica minimizes the molecular degradation of microorganisms during advanced diagenesis. *Chem Geol* 437:98–108.

Allwood AC, Walter MR, Burch IW, *et al*. (2007) 3.43 billion-year-old stromatolite reef from the Pilbara Craton of Western Australia: ecosystem-scale insights to early life on Earth. *Precambrian Res* 158:198–227.

Allwood AC, Rosing MT, Flannery DT, *et al*. (2018) Reassessing evidence of life in 3,700-million-year-old rocks of Greenland. *Nature* 563:241–244.

Aquilano D, Bruno M, and Pastero L (2020) Impurity effects on habit change and polymorphic transitions in the system: Aragonite–Calcite–Vaterite. *Cryst Growth Des* 20:2497–2507.

Balci N, Gunes Y, Kaiser J, *et al*. (2020) Biotic and abiotic imprints on Mg-Rich stromatolites: lessons from Lake Salda, SW Turkey. *Geomicrobiol J* 37:401–425.

Bish DL and Howard SA (1988) Quantitative phase analysis using the Rietveld method. *J Appl Crystallogr* 21:86–91.

Bolton BR, Frakes LA, and Cook JN (1988) Petrography and origin of inversely graded manganese pisolite from Groote Eylandt, Australia. *Ore Geol Reviews* 4:47–69.

Braithwaite CJR and Zedef V (1996) Hydromagnesite stromatolites and sediments in an alkaline lake, Salda Gölü, Turkey. *J Sediment Res* 66:991–1002.

Cady SL, Farmer JD, Grotzinger JP, *et al*. (2003) Morphological biosignatures and the search for life on Mars. *Astrobiology* 3:351–368.

Chan MA, Hinman NW, Potter-McIntyre SL, *et al*. (2019) Deciphering biosignatures in planetary contexts. *Astrobiology* 19:1075–1102.

Clifford SM and Parker TJ (2001) The evolution of the martian hydrosphere: implications for the fate of a primordial ocean and the current state of the Northern Plains. *Icarus* 154: 40–79.

Council TC and Bennett PC (1993) Geochemistry of ikaite formation at Mono Lake, California—implications for the origin of tufa mounds. *Geology* 21:971–974.

Couradeau E, Benzerara K, Gérard E, *et al*. (2013) Cyanobacterial calcification in modern microbialites at the submicrometer scale. *Biogeosciences* 10:5255–5266.

Davies PJ and Bubela B (1973) Transformation of nesquehonite into hydromagnesite. *Chem Geol* 12:289–300.

Dupraz C, Reid RP, Braissant O, *et al*. (2009) Processes of carbonate precipitation in modern microbial mats. *Earth Sci Rev* 96:141–162.

Ehlmann BL, Mustard JF, Murchie SL, *et al*. (2008) Orbital identification of carbonate-bearing rocks on Mars. *Science* 322:1828–1832.

Ehlmann BL, Mustard JF, and Murchie SL (2010) Geologic setting of serpentine deposits on Mars. *Geophys Res Lett* 37: 42596.

Falcón LI, Valdespino-Castillo PM, Alcántara-Hernández RJ, *et al*. (2020) Stromatolites in Crater-Lake Alchichica and Bacalar Lagoon. In *Astrobiology and Cuatro Ciénegas Basin as an Analog of Early Earth*, edited by V. Souza, A. Segura and J.S. Fosters, Springer International Publishing, Switzerland, pp 183–201.

Farley KA, Williford KH, Stack KM, *et al*. (2020) Mars 2020 mission overview. *Space Sci Rev* 216:142.

Farley KA, Stack KM, Shuster DL, *et al*. (2022) Aqueously altered igneous rocks sampled on the floor of Jezero crater, Mars. *Science* 377:eabo2196.

Fassett CI and Head JW (2005) Fluvial sedimentary deposits on Mars: ancient deltas in a crater lake in the Nili Fossae region. *Geophys Res Lett* 32:023456.

Gautier Q, Bénézeth P, Mavromatis V, *et al*. (2014) Hydromagnesite solubility product and growth kinetics in aqueous solution from 25 to 75°C. *Geochim Cosmochim Acta* 138: 1–20.

Gérard E, Ménez B, Couradeau E, *et al*. (2013) Specific carbonate-microbe interactions in the modern microbialites of Lake Alchichica (Mexico). *ISME J* 7:1997–2009.

Gooding JL, Wentworth SJ, and Zolensky ME (1991) Aqueous alteration of the Nakhla meteorite. *Meteoritics* 26:135–143.

Goudge TA, Mustard JF, Head JW, *et al*. (2015) Assessing the mineralogy of the watershed and fan deposits of the Jezero crater paleolake system, Mars. *J Geophys Res planets* 120: 775–808.

Goudge TA, Mohrig D, Cardenas BT, *et al*. (2018) Stratigraphy and paleohydrology of delta channel deposits, Jezero crater, Mars. *Icarus* 301:58–75.

Grotzinger JP and Knoll AH (1999) Stromatolites in Precambrian carbonates: evolutionary mileposts or environmental dipsticks? *Annu Rev Earth Planet Sci* 27:313–358.

Grotzinger JP and Rothman DH (1996) An abiotic model for stromatolite morphogenesis. *Nature* 383:423–425.

Hamilton JL, Wilson SA, Morgan B, *et al*. (2016) Nesquehonite sequesters transition metals and CO_2 during accelerated carbon mineralisation. *Int J Greenhouse Gas Control* 55:73–81.

Hänchen M, Prigiobbe V, Baciocchi R, *et al*. (2008) Precipitation in the Mg-carbonate system—effects of temperature and CO_2 pressure. *Chem Eng Sci* 63:1012–1028.

Haredy RA, Ghandour IM, Erginal AE, *et al*. (2019) Beachrock cementation patterns along the Gulf of Aqaba Coast, Saudi Arabia. *Arab J Sci Eng* 44:479–487.

Harrison AL, Mavromatis V, Oelkers EH, *et al*. (2019) Solubility of the hydrated Mg-carbonates nesquehonite and dypingite from 5 to 35°C: Implications for CO_2 storage and the relative stability of Mg-carbonates. *Chem Geol* 504:123–135.

Harrison AL, Bénézeth P, Schott J, *et al*. (2021) Magnesium and carbon isotope fractionation during hydrated Mg-carbonate mineral phase transformations. *Geochim Cosmochim Acta* 293:507–524.

Hays LE, Graham HV, Marais DJD, *et al*. (2017) Biosignature preservation and detection in Mars analog environments. *Astrobiology* 17:365–400.

Hickman-Lewis K, Cavalazzib B, Fouchera F, *et al*. (2018) Most ancient evidence for life in the Barberton greenstone belt: microbial mats and biofabrics of the ~3.47 Ga Middle Marker horizon. *Precambrian Res* 312:45–67.

Hill RJ and Howard CJ (1987) Quantitative phase analysis from neutron powder diffraction data using the Rietveld method. *J Appl Crystallogr* 20:467–474.

Hopkinson L, Kristova P, Rutt K, *et al*. (2012) Phase transitions in the system MgO-CO_2-H_2O during CO_2 degassing of Mg-bearing solutions. *Geochim Cosmochim Acta* 76: 1–13.

Horgan BHN, Anderson RB, Dromart G, *et al*. (2020) The mineral diversity of Jezero crater: evidence for possible lacustrine carbonates on Mars. *Icarus* 339:113526.

Jones B (2017) Review of calcium carbonate polymorph precipitation in spring systems. *Sediment Geol* 353:64–75.

Kazanci N, Girgin S, and Dügel M (2004) On the limnology of Salda Lake, a large and deep soda lake in southwestern Turkey: future management proposals. *Aquat Conserv* 14: 151–162.

Kaźmierczak J., Kempe S, Kremer B, *et al*. (2011) Hydrochemistry and microbialites of the alkaline crater lake Alchichica, Mexico. *Facies* 57:543–570.

Kennard JM and James NP (1986) Thrombolites and stromatolites: two distinct types of microbial structures. *Palaios* 1: 492–503.

Kloprogge JT, Martens WN, Nothdurft L, *et al*. (2003) Low temperature synthesis and characterization of nesquehonite. *J Mater Sci Lett* 22:825–829.

Knuth JM and Potter-McIntyre SL (2021) Stable isotope fractionation in a cold spring system, Utah, USA: insights for sample selection on Mars. *Astrobiology* 21:235–245.

Koga N, Kasahara D, and Kimura T (2013) Aragonite crystal growth and solid-state aragonite–calcite transformation: a physico–geometrical relationship via thermal dehydration of included water. *Cryst Growth Des* 13:2238–2246.

Koga N and Nishikawa K (2014) Mutual relationship between solid-state aragonite–calcite transformation and thermal dehydration of included water in coral aragonite. *Cryst Growth Des* 14:879–887.

Königsberger E, Königsberger L, and Gamsjager H (1999) Low-temperature thermodynamic model for the system Na_2CO_3-$MgCO_3$-$CaCO_3$-H_2O. *Geochim Cosmochim Acta* 63: 3105–3119.

Lepot K, Compère P, Gérard E, *et al*. (2014) Organic and mineral imprints in fossil photosynthetic mats of an East Antarctic lake. *Geobiology* 12:424–450.

Li J, Benzerara K, Bernard S, *et al*. (2013) The link between biomineralization and fossilization of bacteria: insights from field and experimental studies. *Chem Geol* 359:49–69.

Lin Y, Power IM, and Chen W (2022) Holocene lacustrine abiotic aragonitic ooids from the western Qaidam Basin, Qinghai-Tibetan Plateau. *Minerals* 12:1400.

Lin YJ, Zheng MP, and Ye CY (2017) Hydromagnesite precipitation in the Alkaline Lake Dujiali, central Qinghai-Tibetan Plateau: constraints on hydromagnesite precipitation from hydrochemistry and stable isotopes. *Appl Geochem* 78: 139–148.

Lin YJ, Zheng MP, Ye CY, *et al*. (2019a) Rare earth element and strontium isotope geochemistry in Dujiali Lake, central Qinghai-Tibet Plateau, China: implications for the origin of hydromagnesite deposits. *Geochemistry* 79:337–346.

Lin YJ, Zheng MP, Ye CY, *et al*. (2019b) Trace and rare earth element geochemistry of Holocene hydromagnesite from Dujiali Lake, central Qinghai-Tibetan Plateau, China. *Carbonates Evaporites* 34:1265–1279.

Mandon L, Quantin-Nataf C, Thollot P, *et al*. (2020) Refining the age, emplacement and alteration scenarios of the olivine-rich unit in the Nili Fossae region, Mars. *Icarus* 336:113436.

Mavromatis V, Power IM, Harrison AL, *et al*. (2021) Mechanisms controlling the Mg isotope composition of hydromagnesite-magnesite playas near Atlin, British Columbia, Canada. *Chem Geol* 579:12.

McCutcheon J, Power IM, Harrison AL, *et al*. (2014) A greenhouse-scale photosynthetic microbial bioreactor for carbon sequestration in magnesium carbonate minerals. *Environ Sci Technol* 48:9142–9151.

McCutcheon J, Nothdurft LD, Webb GE, *et al*. (2016) Beachrock formation via microbial dissolution and reprecipitation of carbonate minerals. *Mar Geol* 382:122–135.

McCutcheon J, Power IM, Shuster J, *et al*. (2019) Carbon sequestration in biogenic magnesite and other magnesium carbonate minerals. *Environ Sci Technol* 53:3225–3237.

Michalski JR and Niles PB (2010) Deep crustal carbonate rocks exposed by meteor impact on Mars. *Nat Geosci* 3:751–755.

Ming DW and Franklin WT (1985) Synthesis and characterization of lansfordite and nesquehonite. *Soil Sci Soc Am J* 49: 1303–1308.

Mook WG, Bommerson JC, and Staverman WH (1974) Carbon isotope fractionation between dissolved bicarbonate and gaseous carbon dioxide. *Earth Planet Sci Lett* 22:169–176.

Morris RV, Ruff SW, Gellert R, *et al*. (2010) Identification of carbonate-rich outcrops on Mars by the Spirit Rover. *Science* 329:421–424.

Niles PB, Catling DC, Berger G, *et al*. (2013) Geochemistry of carbonates on Mars: implications for climate history and nature of aqueous environments. *Space Science Rev* 174:301–328.

Noffke N, Christian D, Wacey D, *et al*. (2013) Microbially induced sedimentary structures recording an ancient ecosystem in the ca. 3.48 billion-year-old Dresser Formation, Pilbara, Western Australia. *Astrobiology* 13:1103–1124.

O'Neil JR and Barnes I (1971) C^{13} and O^{18} compositions in some fresh-water carbonates associated with ultramafic rocks and serpentinites: western United States. *Geochim Cosmochim Acta* 35:687–697.

Parkhurst DL and Appelo CAJ (2013) Description of input and examples for PHREEQC Version 3—a computer program for speciation, batch-reaction, one-dimensional transport, and inverse geochemical calculations. In *US Geological Survey Techniques and Methods*, Denver, Colorado, pp 497.

Power IM, Wilson SA, Thom JM, *et al* (2007) Biologically induced mineralization of dypingite by cyanobacteria from an alkaline wetland near Atlin, British Columbia, Canada. *Geochem Trans* 8:13.

Power IM, Wilson SA, Thom JM, *et al*. (2009) The hydromagnesite playas of Atlin, British Columbia, Canada: a biogeochemical model for CO_2 sequestration. *Chem Geol* 260: 286–300.

Power IM, Dipple GM, and Southam G (2010) Bioleaching of ultramafic tailings by *Acidithiobacillus* spp. for CO_2 Sequestration. *Environ Sci Technol* 44:456–462.

Power IM, Wilson SA, Dipple GM, *et al*. (2011) Modern carbonate microbialites from an asbestos open pit pond, Yukon, Canada. *Geobiology* 9:180–195.

Power IM, Wilson SA, Harrison AL, *et al*. (2014) A depositional model for hydromagnesite–magnesite playas near Atlin, British Columbia, Canada. *Sedimentology* 61:1701–1733.

Power IM, Harrison AL, and Dipple GM (2016) Accelerating mineral carbonation using carbonic anhydrase. *Environ Sci Technol* 50:2610–2618.

Power IM, Harrison AL, Dipple GM, *et al*. (2019) Magnesite formation in playa environments near Atlin, British Columbia, Canada. *Geochim Cosmochim Acta* 255:1–24.

Power IM, Paulo C, Long H, *et al*. (2021) Carbonation, cementation, and stabilization of ultramafic mine tailings. *Environ Sci Technol* 55:10056–10066.

Preston LJ, Shuster J, Fernández-Remolar D, *et al*. (2011) The preservation and degradation of filamentous bacteria and biomolecules within iron oxide deposits at Rio Tinto, Spain. *Geobiology* 9:233–249.

Renaut RW (1993) Morphology, distribution, and preservation potential of microbial mats in the hydromagnesite-magnesite playas of the Cariboo Plateau, British Columbia, Canada. *Hydrobiologia* 267:75–98.

Riding R (2000) Microbial carbonates: the geological record of calcified bacterial-algal mats and biofilms. *Sedimentology* 47: 179–214.

Rietveld HM (1969) A profile refinement method for nuclear and magnetic structures. *J Appl Crystallogr* 2:65–71.

Robles-Fernández A, Areias C, Daffonchio D, *et al*. (2022) The Role of microorganisms in the nucleation of carbonates, environmental implications and applications. *Minerals* 12: 1562.

Romanek CS, Grossman EL, and Morse JW (1992) Carbon isotopic fractionation in synthetic aragonite and calcite—effects of temperature and precipitation rate. *Geochim Cosmochim Acta* 56:419–430.

Ruiz-Agudo E, Putnis CV, and Putnis A (2014) Coupled dissolution and precipitation at mineral–fluid interfaces. *Chem Geol* 383:132–146.

Russell MJ, Ingham JK, Zedef V, *et al*. (1999) Search for signs of ancient life on Mars: expectations from hydromagnesite microbialites, Salda Lake, Turkey. *J Geol Soc London* 156: 869–888.

Saldi GD, Jordan G, Schott J, *et al*. (2009) Magnesite growth rates as a function of temperature and saturation state. *Geochim Cosmochim Acta* 73:5646–5657.

Saldi GD, Schott J, Pokrovsky OS, *et al*. (2012) An experimental study of magnesite precipitation rates at neutral to alkaline conditions and 100–200 degrees C as a function of pH, aqueous solution composition and chemical affinity. *Geochim Cosmochim Acta* 83:93–109.

Salese F, Pondrelli M, Neeseman A, *et al*. (2019) Geological evidence of planet-wide groundwater system on Mars. *J Geophys Res Planets* 124:374–395.

Scheller EL, Swindle C, Grotzinger J, *et al*. (2021) Formation of magnesium carbonates on Earth and implications for Mars. *J Geophys Res Planets* 126:32.

Schopf JW, Kudryavtsev AB, Czaja AD, *et al*. (2007) Evidence of archean life: stromatolites and microfossils. *Precambrian Res* 158:141–155.

Shirokova LS, Mavromatis V, Bundeleva IA, *et al*. (2013) Using mg isotopes to trace cyanobacterially mediated magnesium carbonate precipitation in alkaline lakes. *Aquat Geochem* 19:1–24.

Sugitani K, Lepot K, Nagaoka T, *et al*. (2010) Biogenicity of morphologically diverse carbonaceous microstructures from the ca. 3400 Ma Strelley pool formation, in the Pilbara Craton, Western Australia. *Astrobiology* 10:899–920.

Sun Y, Li YL, Li L, *et al*. (2019) Preservation of cyanobacterial UVR-shielding pigment scytonemin in carbonate ooids formed in Pleistocene salt lakes in the Qaidam Basin, Tibetan Plateau. *Geophys Res Lett* 46:10375–10383.

Tait AW, Wilson SA, Tomkins AG, *et al*. (2017) Evaluation of meteorites as habitats for terrestrial microorganisms: results from the Nullarbor Plain, Australia, a Mars analogue site. *Geochim Cosmochim Acta* 215:1–16.

Tait AW, Wilson SA, Tomkins AG, *et al*. (2022) Preservation of terrestrial microorganisms and organics within alteration products of chondritic meteorites from the Nullarbor Plain, Australia. *Astrobiology* 22:399–415.

Tarnas JD, Stack KM, Parente M, *et al*. (2021) Characteristics, origins, and biosignature preservation potential of carbonate-bearing rocks within and outside of Jezero crater. *J Geophys Res Planets* 126:e2021JE006898.

Tarutani T, Clayton RN, and Mayeda TK (1969) The effect of polymorphism and magnesium substitution on oxygen isotope fractionation between calcium carbonate and water. *Geochim Cosmochim Acta* 33:987.

Tavera R and Komárek J (1996) Cyanoprokaryotes in the volcanic lake of Alchichica, Puebla State, Mexico. *Algol Stud* 83:511–538.

Vago JL, Westall F, and Cavalazzi B (2019) Searching for signs of life on other planets: Mars a case study. In: *Biosignatures for Astrobiology*, edited by B. Cavalazzi and F. Westalls, Springer International Publishing, Cham, pp 283–300.

Valdespino-Castillo PM, Alcántara-Hernández RJ, Alcocer J, *et al*. (2014) Alkaline phosphatases in microbialites and bacterioplankton from Alchichica soda lake, Mexico. *FEMS Microbiol Ecol* 90:504–519.

Vázquez-Nion D, Silva B, and Prieto B (2018) Influence of the properties of granitic rocks on their bioreceptivity to subaerial phototrophic biofilms. *Sci Tot Environ* 610–611: 44–54.

Walsh MM (1992) Microfossils and possible microfossils from the Early Archean Onverwacht Group, Barberton Mountain Land, South Africa. *Precambrian Res* 54:271–293.

Westall F, Foucher F, Bost N, *et al*. (2015) Biosignatures on Mars: What, where, and how? Implications for the search for martian life. *Astrobiology* 15:998–1029.

White RA, Power IM, Dipple GM, *et al*. (2015) Metagenomic analysis reveals that modern microbialites and polar microbial mats have similar taxonomic and functional potential. *Front Microbiol* 6:14.

Wilson SA, Dipple GM, Power IM, *et al*. (2009) Carbon dioxide fixation within mine wastes of ultramafic-hosted ore deposits: examples from the Clinton Creek and Cassiar chrysotile deposits, Canada. *Econ Geol* 104:95–112.

Wilson SA, Barker SLL, Dipple GM, *et al*. (2010) Isotopic disequilibrium during uptake of atmospheric CO_2 into mine process waters: implications for CO_2 sequestration. *Environ Sci Technol* 44:9522–9529.

Wray JJ, Murchie SL, Bishop JL, *et al*. (2016) Orbital evidence for more widespread carbonate-bearing rocks on Mars. *J Geophys Res Planets* 121:652–677.

Xiao L, Wang J, Dang YN, *et al*. (2017) A new terrestrial analogue site for Mars research: the Qaidam Basin, Tibetan Plateau (NW China). *Earth Sci Rev* 164:84–101.

Xu XC, Guo HX, Li M, *et al*. (2021) Bio-cementation improvement via $CaCO_3$ cementation pattern and crystal polymorph: a review. *Constr Build Mater* 297:16.

Zastrow AM and Glotch TD (2021) Distinct carbonate lithologies in Jezero Crater, Mars. *Geophys Res Lett* 48: e2020GL092365.

Zeyen N, Benzerara K, Beyssac O, *et al*. (2021) Integrative analysis of the mineralogical and chemical composition of modern microbialites from ten Mexican lakes: what do we learn about their formation? *Geochim Cosmochim Acta* 305: 148–184.

Address correspondence to:
Ian M. Power
Trent School of the Environment
Trent University
1600 West Bank Drive
Peterborough, ON K9L 0G2
Canada

E-mail: ianpower@trentu.ca

Submitted 18 August 2022
Accepted 16 February 2023

Abbreviations Used

CRISM = Compact Reconnaissance Imaging Spectrometer for Mars
EDS = energy dispersive spectrometer
HMDS = hexamethyldisilazane
SEM = scanning electron microscopy
SI = saturation index
UV = ultraviolet
VPDB = Vienna Pee Dee Belemnite
VSMOW = Vienna Standard Mean Ocean Water
XRD = X-ray diffractometer